Experimental Analysis of Pressure Shielding Mechanisms in Bio-Inspired Unidirectional Canopies

Nandita Nurani Hari *, Máté Szőke† and William J. Devenport‡
Kevin T Crofton Department of Aerospace and Ocean Engineering, Virginia Tech, Blacksburg, VA 24061, USA

Stewart Glegg§
Department of Ocean and Mechanical Engineering, Florida Atlantic University, Boca Raton, FL 33431, USA

Previous studies have demonstrated that treatments such as a canopy or finlets placed within a boundary layer can shield surfaces from unsteady pressure fluctuations without substantially compromising the aerodynamic performance. This paper describes research into fundamental mechanisms of this phenomenon known as pressure shielding. Unidirectional canopy is an idealised surface treatment which consists of streamwise array of rods cantilevered at the downstream end, inspired from the downy coating on owls' wings. Experiments show that such a canopy attenuates the surface pressure in two distinct frequency ranges. At low frequencies associated with convective scales much greater than the canopy height, the attenuation spectra show scaling on Strouhal number based on canopy height. At high frequencies, associated with convective scales of the order of canopy height or lower, a dissipation type frequency scaling appears more appropriate. The ratio of streamwise distance over the height is an important parameter at the low frequency regions of attenuation, while the open-area ratio controls the broadband magnitude of attenuation spectra. Spatial and temporal correlations further shed light on the effects of the canopy in reducing the larger, energetic turbulent structures associated with the wall jet unsteady surface pressure fluctuations.

Nomenclature

d = Canopy rod diameter

*Graduate Research Assistant and Student Member AIAA
†Senior Research Fellow and Member AIAA
‡Professor and Associate Fellow AIAA
§Professor and Associate Fellow AIAA

Presented as a conference paper in AIAA Scitech 2021, Virtual, 11th-15th January 2021, Paper number: 2021-0817

S	=	Canopy rod spacing measured between two adjacent rod centers
h	=	Canopy height from wall
f	=	Frequency
U	=	Velocity scale
U_m	=	flow speed at boundary layer height
U_j	=	Wall jet speed
x	=	streamwise distance measured from the canopy leading edge
Re_j	=	Reynolds number based on the wall jet nozzle height
Rex	=	Reynolds number based on x
δ	=	boundary layer thickness
δ^*	=	boundary layer displacement thickness
θ	=	boundary layer momentum thickness
A_u, A_D, B, A	=	Wygnanski et al. [1] constants for the wall jet
τ	=	time-delay
Δx	=	streamwise separations
U_c	=	Convection velocity of surface pressure fluctuations
λ_z	=	Spanwise correlation lengthscale
γ^2	=	coherence
OAR	=	Open-area ratio
U_1, U_2	=	streamwise and vertical mean velocity, respectively
u_1, u_2	=	streamwise and vertical turbulent quantities respectively

I. Introduction

Surface pressure fluctuations originating from turbulent flows over surfaces act as excitation for major sources of flow noise such as the trailing edge noise that dominates from wind turbines [2–4] and leading edge noise of helicopter rotors [5, 6]. They also potentially contaminate measurements made with surface-mounted instrumentation which play an important role in active flow control, environmental monitoring [7, 8] and surveillance applications [9, 10]. Surface pressure fluctuations drive the fluid structure interactions which are of significance in panel vibration noise sources such as cabin noise and interior wind noise in cars [11, 12]. On an atmospheric scale, surface pressure fluctuations are directly related to wind gust magnitude that can cause damage to structures [13–15]. With expansion of the aviation industry, there is an increased attention towards noise reducing technologies in aircraft. Aerodynamic noise becomes a major contributor especially during taking-off and landing. With growing global renewable energy requirements, there is a potential increase in wind turbine diameter and development of large-scale farms leading to higher noise pollution levels especially for the nearby residents. Studies [16, 17] suggest use of passive control devices such as brushes [18], serrations [19, 20] and porous surfaces [21, 22] to address the broadband trailing edge generated in a modern horizontal axis wind turbine. Therefore, control of wall-bounded turbulent boundary layer flows is both technologically desirable and an interesting scientific problem in different aero-hydrodynamic applications.

Background

Owls are known for their extremely quiet flight owing to a combination of features on their wings discovered initially by Graham [23]. Early studies on the aerodynamics and acoustics of owls flight by Thorpe and Griffin [24] and Kroeger et al. [25] found significantly lower noise levels compared to other birds especially at frequencies above 2 kHz. Graham [23] revealed three unique features include first, evenly spaced bristles along the wing leading edge, second, fringes along the trailing edge and finally, velvety covering over the upper wing surface and a downy lower surface as studied by Kroeger et al. [25]. Lilley [26] studied the owl wings extensively and established that the presence of the velvety coating dampens turbulence within the boundary layer thus eliminating broadband sound generation. Jaworski and Peake [27] give a detailed view on the various treatments that are inspired by owls' silent flight.

The objective of this study is to deal with the turbulent boundary layer noise, which is caused due to the interaction of turbulence with the surface. The unsteady pressure in the hydrodynamic wavenumber range is scattered as sound in the acoustic wavenumber range [28]. Based on findings of Lilley [26], flow noise generated from turbulent flow over aerodynamic surfaces could be reduced by manipulating the boundary layer and thus the source itself. Clark et al. [29] developed practical bio-inspired surface treatments based on owls' downy coating which exhibit reduction in surface pressure fluctuations. They tested different fabric canopies over rough surfaces and studied the surface pressure fluctuations and the far-field acoustics. The fabric canopies show reduction in surface fluctuations predominantly in the mid and high frequency regions. They further developed unidirectional canopies with an open area ratio of 70% mimicking that of an owl, made using fishing lines, to eliminate the self-noise generated by the flow interacting with the cross-threads. These showed significant effect in reducing the surface pressure fluctuations up to 30 dB and a maximum reduction of 6 dB in the far-field levels. The attenuation of the surface fluctuations reduces with increase in canopy scale and Reynolds number of the flow. The pressure attenuation showed an exponential growth, modeled as a function of its frequency, based on the hypothesis that the canopy introduces a new shear layer that displaces the generation of pressure-producing instabilities away from the wall [29].

The practical advantage of using surface treatments to attenuate surface pressure fluctuations opened up research to design and implementation of pressure shielding techniques [10]. Computational analysis of finlets [30–32] shows reduction in flow velocities between the fins and the turbulent kinetic energy near the walls. The turbulent kinetic energy however seemed to increase at the height of the finlets. The resulting pressure fluctuations are attenuated exponentially with streamwise distance below the canopy, effectively shielding the wall. Afshari et al. [20], Millican et al. [33], Afshari et al. [34, 35] analyzed practical designs inspired from unidirectional canopy measurements [29] which showed velocity deficit up to the height of the treatments. This led to hypothesizing that one of the dominant mechanisms controlling the interaction of the treatments with the flow is shear sheltering [36]. Jimenez et al. [37] showed the change in the mean velocity profile introduced by the canopy has a significant effect on the unsteady surface pressure fluctuations. Afshari et al. [20] showed an inflection in the mean and increase in turbulent kinetic energy profiles with increasing finlet height and reduction in the spacing. The turbulent structures showed a reduction near the wall with increasing height and spacing.

The studies mentioned above show a consistent picture of pressure shielding, however, the

fundamental understanding of the mechanisms is still not completely understood. The interaction of the surface treatments with the flow and the resultant effect on the surface pressure is unclear. This paper is an expansion of the work presented in Nurani Hari et al. [38]. In this study, a unidirectional canopy has been used for analyzing the effect of surface treatments on the unsteady wall pressure fluctuations. Such a canopy design represents an idealized surface treatment without any leading edge effect to simulate study of canopies on the surface pressure fluctuations. The objective of this paper is to better understand how these surface treatments fundamentally work. This has been done by examining the characteristics of surface pressure attenuation of the canopies, the effect of variation in the flow and geometric parameters on the attenuation. Finally, the effects on the space-time pressure correlations by canopies have been revealed.

II. Experimental Setup and Instrumentation

The experiments shown as a part of this effort were performed in the Anechoic Wall-jet facility at Virginia Tech. It is an arrangement with flow exhausting from a nozzle over a surface at laboratory scale with no significant edge noise and a jet boundary suitable for in-flow and far-field acoustic measurements in an anechoic environment [1], [39], [40]. The wall jet flow is a fundamentally complex, instantaneously three-dimensional flow creating a region of boundary layer near the wall and a shear layer in the outer region. The two distinct regions studied by Gersten [41], George et al. [42], Katz et al. [43], comprises the inner region with some of the near-wall characteristics of a boundary layer and the second, an outer layer formed from the mixing of the high momentum jet with the quiescent air. The flow in the facility develops into self-similar profiles as it moves downstream as shown by Kleinfelter et al. [44]. Turbulent plane wall jet flows also replicate various engineering applications such as boundary layer development over surfaces, airfoils, blades and combustion chambers [1].

A. Anechoic wall jet wind tunnel Facility

Figure 1 is the schematic showing cross-section of the Anechoic wall jet facility. The earlier version of the facility was built in 2007 [45] and was extensively used to study roughness noise [46–48], boundary layer flows over steps [49], flow over acoustically treated surfaces [46]. It was later re-designed and developed to a new facility in 2019 to increased the operational life and accessibility [44]. The jet flow from the nozzle exhausts over a flat plate and develops into a fully developed, self-similar turbulent boundary layer flow. The mean flow velocity gradually decreases with streamwise distance as it loses energy to the ambient. The coordinate system originates at a streamwise distance of 1.28 m from the nozzle exit which corresponds to the leading edge of the canopy structure discussed in detail in the following section. Positive $x-$axis is along the streamwise direction, y is the vertical axis with positive away from the wall and z is the spanwise coordinate shown in Fig 2b) and 3. The tests were run in the wall jet wind tunnel facility at Reynolds number, $U_m\delta/\mu$ of 6x10^3 - 12x10^3 measured at the canopy leading edge. The air is issued over the plate which is enclosed in a large anechoic chamber with provision to install aerodynamic and aeroacoustic testing rigs. The turbulent flow in our case develops over a wide wall-plate ensuring spanwise uniformity Kleinfelter et al. [44]. Such a flow reduces to a two-dimensional mean flow which

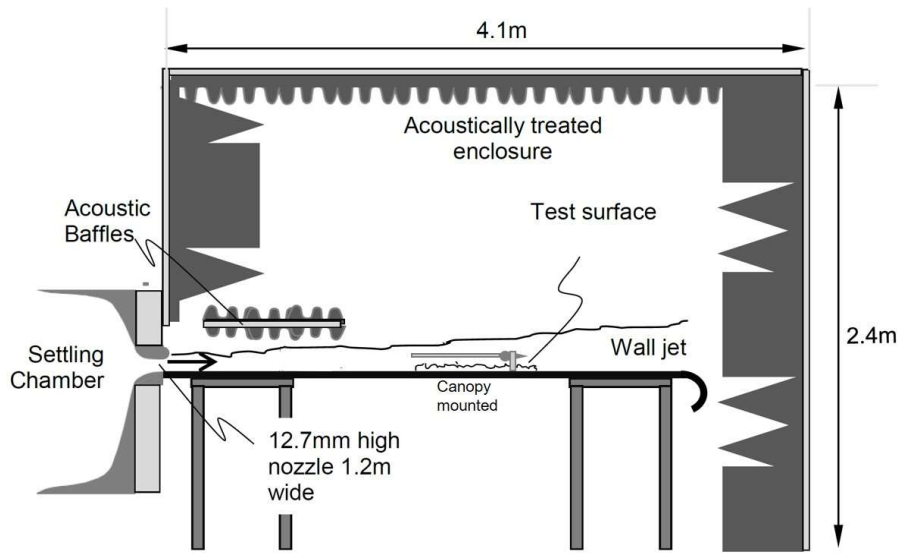

Fig. 1 Schematic of the cross-sectional view of the Anechoic wall jet facility at Virginia Tech

allows us to predict the boundary layer parameters using algebraic relations [1]. Mean profiles at different streamwise locations starting from x of -152.4 mm were measured to study the flow evolution. Tests were performed for jet speeds ranging from 20-70 m/s. [44] also demonstrated spanwise uniformity in the wall jet facility between z of -400 mm to 400 mm, especially enclosing the test-section between z of -254 mm to 254 mm. Flow at the most upstream location corresponding to the test-plate leading edge, x of -152.4 mm, shows higher uncertainty of $U_1/U_j = \pm 0.025$. The measured data was used in the wall jet boundary layer relations given by Wygnanski et al. [1] to predict the appropriate coefficients for the facility. The relations are given by,

$$\frac{U_m}{U_j} = A_U Re_j^{n+1} Re_x^n \tag{1}$$

$$\frac{\delta^*}{h_j} = A_D Re_j^{p-2} Re_x^p \tag{2}$$

$$\theta = B\delta^* \tag{3}$$

$$\delta = A\delta^* \tag{4}$$

where, U_j is the jet velocity, δ^* is the displacement thickness, θ is the momentum thickness, δ is the boundary layer thickness and U_m is the maximum velocity in the boundary layer. Re_j and Re_x are the Reynolds numbers based on nozzle height and streamwise distance respectively. Constants A_U, A_D, A, B, n and p were determined from wall jet mean velocity measurements for the facility [44]. Given these constants, we can predict the boundary layer parameters at any downstream location. The friction velocity, u_τ is computed using empirical relations given by [42] for wall jet.

Reference conditions

The jet exit velocity was measured at the nozzle exit by measuring dynamic pressure based on total pressure in the settling chamber and ambient pressure inside the test chamber. Tygon tubes from both locations are connected to ±3.75 kPa-range Setra 239 pressure transducer that reads a differential pressure with an uncertainty of $\pm 2.5V$. This transducer was connected to an NI-DAQ which fed data to an in-house MATLAB program. Atmospheric pressure was provided from local meteorological conditions, corrected for the appropriate elevation. Flow temperature was measured with a thermocouple connected to Omega DP86T analog output with an uncertainty estimated to be 0.1^oC.

B. Canopy configurations

The canopy treatments designed consist of evenly spaced arrays of rods placed streamwise to recreate the essential features of unidirectional canopies tested by Clark et al. [29] as shown in Figure 2, 3. Rods were chosen over previously used fibers because they can be cantilevered from downstream thereby eliminating influence of any leading edge structure. The airfoil support structure of the canopy rods is mounted on 50 mm x 50 mm of L-brackets manufactured from 1 mm thick metal sheet so as to have a forward projected area of only 38 mm^2. Overall span of the airfoil is 254 mm for canopies A-C and F (see Table 1) and 305 mm for canopies D and E. Multiple geometric parameters such as the diameter (d), spacing (S) and height (h) of the canopy rods can be altered, making it possible to analyze the effect of different non-dimensional parameters independently. Spacing, S is defined as the distance between the mid-points of two consecutive rods (center-to-center). The gap between the two rods is then given by $s \equiv S - d$. The height, h is measured as the vertical distance from the center of the rods to the wall. The open area ratio (OAR) given by $s/(s+d)$, ratio of effective open-area and the total area, is a crucial parameter used to characterize the canopy. Rods were smoothed at the tips and push-fit into the airfoil support at an offset of 2.54 mm below the airfoil center-line. The airfoil support is designed to be aerodynamic to ensure minimal disturbance to the flow. A McMasters Henderson airfoil, was chosen due to its good aerodynamic performance and low aeroacoustic self-noise [50]. The airfoil chord and thickness are 40 mm and 6.35 mm respectively, and the leading edge of the airfoil was positioned nearly 254 mm downstream of the canopy leading edges. Potential flow calculations showed that the upstream disturbance of the airfoil was less than 5% of velocity at distances further than $5h$ upstream of its leading edge.

Different canopy configurations tested are given in Table 1. They were tested for different heights from the wall ranging between 2 - 15 mm. The open-area ratio in in the range of 65-88% for all the canopies tested, closely representing the canopy designed by Clark et al. [29]. All tested configurations are placed such that the leading edge of the canopy is 1.28 m from the nozzle exit of the wall jet wind tunnel facility. The mean flow here has a fully developed turbulent boundary layer profile [44].

C. Surface pressure measurements

Measurement of the surface pressure spectra was done with Knowles electret microphones (FG-23329-P07) mounted flush to the wall. These microphones have a circular sensing area of

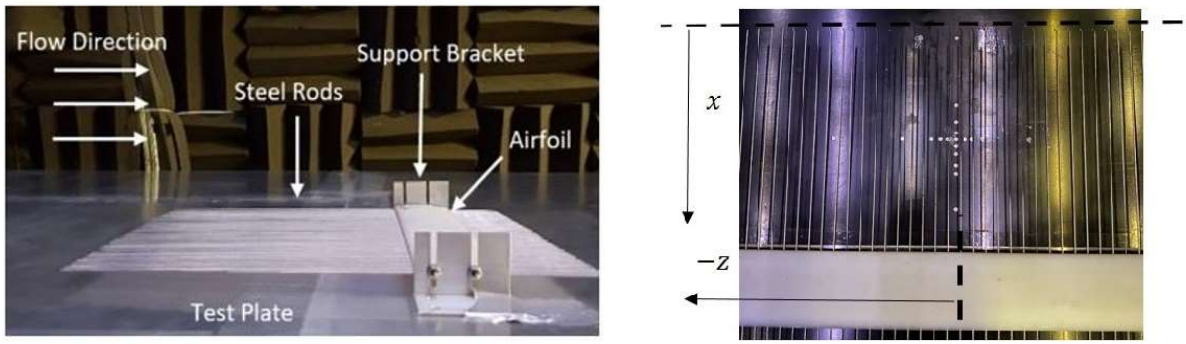

Fig. 2 (Left) Canopy oriented in the streamwise direction placed parallel to the wall. (Right) Planform view of the canopy placed over the surface microphone array [38]

Canopy configurations	d (mm)	S (mm)	Open Area Ratio, $s/(s+d)$	h (mm)
A	1	3	0.66	2,4,6,8,12,15
B	1.56	4.68	0.66	2,4,6,8,12,15
C	1	4	0.75	2,4,6,8,12,15
D	2	6	0.66	6,8,12,15
E	2	9	0.66	6,8,12
F	1	8	0.88	6,8,12,15

Table 1 Geometric parameters of different canopy configurations tested

0.76 mm^2, with a flat frequency response between 100 Hz-10 kHz. Surface pressure fluctuations were measured at eight downstream locations at $z = 0$ along mid-span of the canopy to capture the downstream evolution of attenuation. Figure 3 shows the experimental setup consisting of a horizontal canopy placed at height h, with undisturbed flow profile at canopy leading edge. The canopy was placed such that microphones were centered spanwise in the gap between two adjacent rods of the canopy. Figure 3 shows the streamwise and spanwise microphone array respectively below the canopy with the streamwise microphones starting from the canopy leading edge and extending to 127 mm downstream. The distance of each streamwise microphone (along x) is measured from the canopy leading edge. The spanwise array at 76.2 mm downstream from the canopy leading edge and extends to up to 86 mm in the $-z$ direction. The distance of spanwise microphones are measured from the $z = 0$ axes.

The Knowles microphones were calibrated prior to the experiments against a B&K Type 4138 1/8-in microphone of known response. The calibration procedure was as follows. An ID60C8 speaker was used to emit white noise 1700 mm away from the microphone location, and the entire setup was placed inside an anechoic chamber. Sensitivity of the reference B&K microphone was determined by pistonphone calibration at 251.2 Hz. Microphone data was acquired using six-channel Bruel and Kjaer Type 3050 24-bit LAN-XI module sampled at 65536 Hz. To process the time

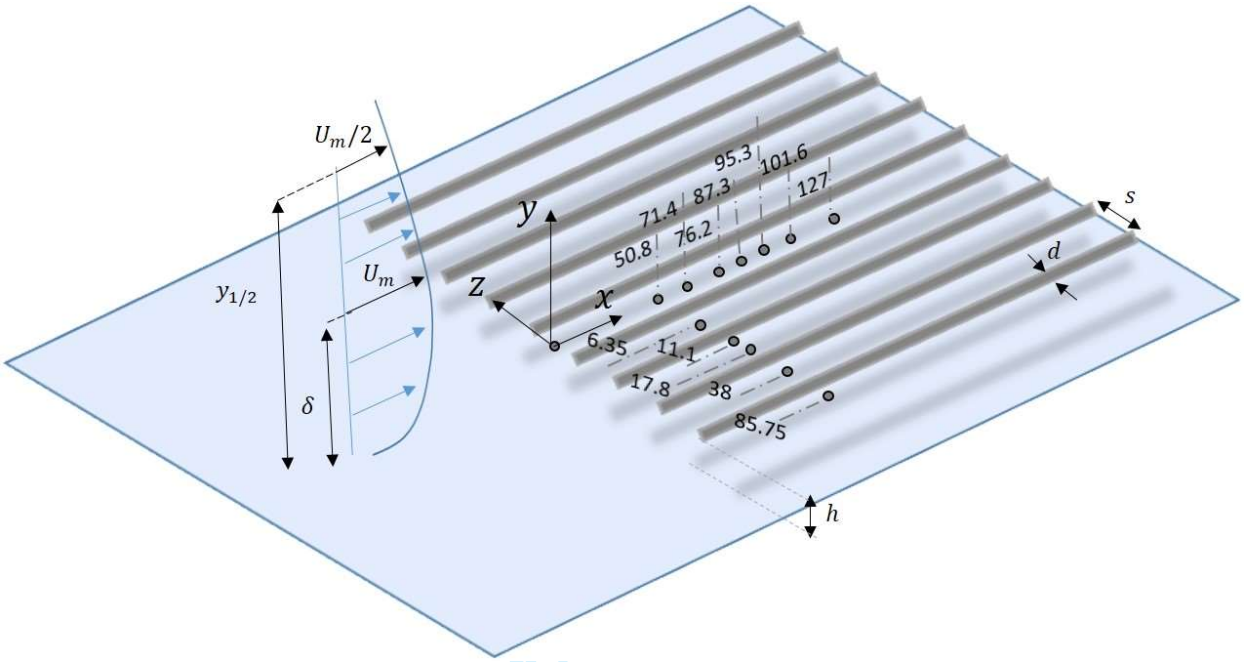

Fig. 3 Schematic of the unidirectional canopies placed in the wall jet turbulent boundary layer. The streamwise microphone array is along the $z = 0$, starting at the canopy leading edge. The spanwise microphone array is along the $-z$ direction, measured from the mid-span. All the distances are in mm.

series data, Fast Fourier Transform of the data was performed for sections of records of length 8192 multiplied by a Hanning Window with 50% overlap. Absolute pressure fluctuation levels are presented in units dB/Hz defined by $10\log_{10}(G_{\mathrm{pp}}/p_{ref}^2)$, where G_{pp} is the one-sided spectral density and p_{ref} is 20μPa/Hz. The attenuation in surface pressure fluctuations is obtained by subtracting canopy pressure fluctuation (G_{pp_c}) from the untreated , no-canopy or baseline wall jet surface pressure spectra (G_{pp_b}) given by, $10\ \log_{10}(G_{\mathrm{pp}_b}/G_{\mathrm{pp}_c})$. Uncertainty in the measured pressure spectral density was obtained to be highest value of 0.8 dB at frequencies below 200 Hz and reducing to 0.5 dB at frequencies above 6 kHz. This uncertainty is calculated based on the spectral analysis of the calibrated pressure data therefore also includes the uncertainty in the measurement arising from microphone calibrations. Additionally accounting for uncertainties due to microphone placement, flow conditions etc., repeated measurements showed a total uncertainty of nearly 1 dB. The uncertainty in the attenuation spectra is calculated to be highest value of 1.2 dB at frequencies below 200 Hz and lowering to 0.8 dB at frequencies above 6 kHz.

D. Flow characteristics in the wall jet and around canopies

Recent experimental studies to determine flow in smooth wall jet have been performed using 2D Time-Resolved Particle Image Velocimetry (TR-PIV) [51, 52]. Canopy D with an open area ratio of 66% and h = 6 mm was chosen as a representative case because it provides a larger gap between the rods for laser sheet placement and also produces significant broadband attenuation. This

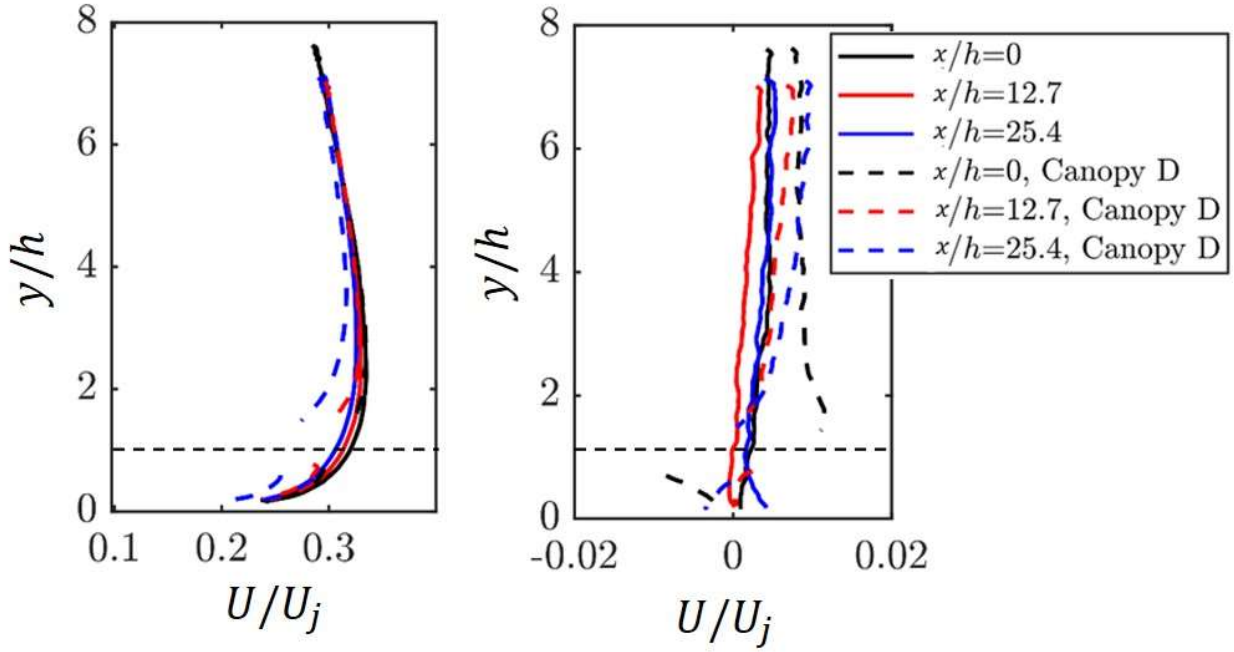

Fig. 4 Mean velocity in the streamwise (U_1) and vertical (U_2) evolution along three streamwise locations at U_j = 50 m/s, obtained using planar, Time-Resolved PIV. Profiles are plotted for the untreated (solid lines) and canopy D (dashed lines) at height, h = 6 mm [51]

section gives an overview of the mean flow results for the clean-wall (untreated) case and canopy D. Detailed description of the PIV measurements and results are given in [51]. Figure 4 shows the streamwise and vertical mean flow velocity profiles for untreated and canopy D at height, h of 6 mm for a jet speed of 50 m/s. The flow velocities are normalized by the jet speed, U_j and the vertical distances are normalized by the canopy height, h, which is 6 mm in this case. Profiles at three streamwise locations correspond to x of 0 mm, 76.2 mm and 152.4 mm from the canopy leading edge location. At the canopy leading edge, flow profiles are similar for the untreated(clean-wall) and canopy cases. Differences start to emerge as we move downstream. The most downstream location in Figure 4 shows a significant reduction in the streamwise mean flow both below and above the canopy rods. The boundary layer parameters obtained for the two jet speeds are shown at x = 0 m in the Table 2 below. Figure 5 shows the normalized streamwise, $\overline{u_1u_1}$, wall-normal, $\overline{u_2u_2}$ and Reynolds turbulent stress, $\overline{u_1u_2}$ profiles for untreated (solid-lines) and canopy D (dashed-lines) at h = 6 mm and U_j of 50 m/s at three different streamwise locations. For the prior PIV studies, the measurements started from a wall distance of y^+ of 40, therefore the near-wall viscous region is not captured. The three turbulence components for the untreated flow increase with vertical distance from the wall. $\overline{u_1u_1}$ has the largest magnitude among the three components as is common for streamwise turbulent flows. The streamwise turbulence intensity decays as we move downstream since the jet loses momentum to the surrounding. The results for the canopy show reduction in levels of all three turbulence components below the canopy height. Above the canopy at $y > 1.5h$ the streamwise turbulence shows an increase in magnitude which is similar to the observation made in

	U_j = 30m/s	U_j =50m/s
U_m(m/s)	9.85	16.74
δ(m)	0.0171	0.0146
δ^*(m)	0.015	0.0011
θ(m)	0.0011	0.0008
u_τm/s	0.5203	0.8582
$y_{1/2}$(m/s)[estimated]	0.1058	0.1021

Table 2 Wall jet Boundary layer parameters calculated at the leading edge location of the canopy for jet velocities, U_j of 30 m/s and 50 m/s using PIV

finlets [33]. The canopy seems to increase the streamwise turbulence at certain frequencies and this is accompanied by dampening of vertical turbulence. The reduction in $\overline{u_2u_2}$ is observed both below the rods and above up to 2-3h due to blocking of vertical momentum by the canopy rods similar to observation in plant canopies by Finnigan [14]. $\overline{u_1u_2}$ reduces above the canopy at distances up to 2h and an increase in the region below canopy which is possibly associated with increase in friction by canopy rods causing the flow to decelerate below the canopy.

E. Parametric study of the flow domain

For a canopy placed in a turbulent boundary layer, the pressure is expected to have a functional form based on flow and geometric parameters given by,

$$p' = f(p'_b, U_h, U_m, \delta, \nu, S, d, h, x, f...) \tag{5}$$

Where, p_b is the untreated surface pressure, U_h is the mean flow velocity at the canopy leading edge, measured at the height of the canopy. δ and U_m is obtained from the PIV measurements. S, d, h and x are geometric parameters of the canopy design and configuration, shown in Fig 3. Based on these parameters, we can predict some meaningful non-dimensional parameters,

$$p'/(p'_b) = f(\frac{x}{h}, \frac{s}{s+d}, \frac{d}{h}, \frac{f\nu}{U_m^2}, \frac{fh}{U_m}, \frac{\delta}{h}) \tag{6}$$

x/h represents the streamwise distance normalized over the height and this is a crucial parameter governing the leading edge development of attenuation Gonzalez et al. [53]. $S/(S+d)$ represents the permeability of the canopy to vertical transfer of momentum, d/h represents the blockage experienced by the flow and appears to govern the intensity of attenuation at all frequencies. $f\nu/U_m^2$ represents the dissipation scaling which we hypothesize to govern the high-frequency spectra. fh/U_m is the Strouhal number based on the height of the canopy and δ/h is the ratio of boundary layer thickness and canopy height.

We observe, consistent with prior studies where the velocity field has been examined, that the incoming flow is slowed down below the canopy due to friction by both the canopy and the wall surfaces, while the mean streamwise flow above the canopy remains largely unchanged. The slowing

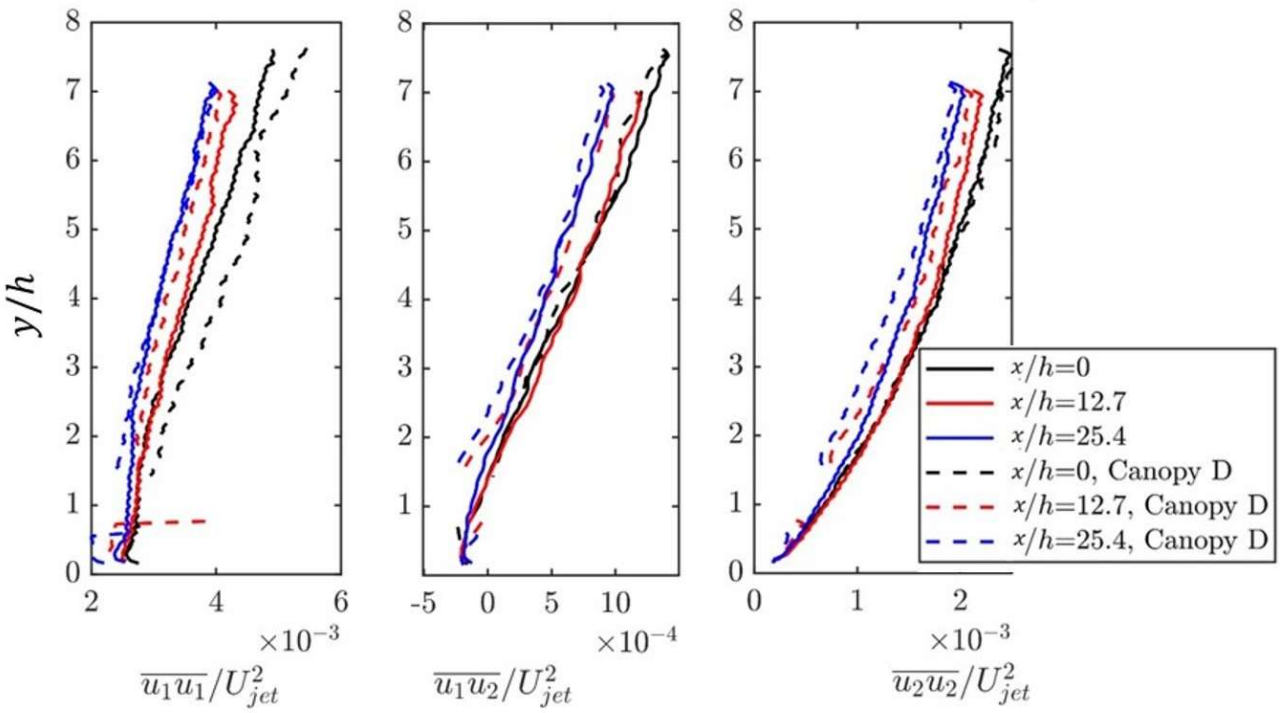

Fig. 5 Streamwise, wall-normal and Reynolds turbulent stresses for the clean wall configuration(solid) and the canopy D(dashed) at height, h = 6 mm, for the U_j = 50 m/s

of the velocity beneath the canopy could be possibly causing reduction in the near-wall mean velocity gradient and the flow turbulent energy, therefore having an implication on the surface pressure. An increase in the canopy open-area ratio is hypothesized to reduce the attenuation magnitude. The following sections attempt to experimentally analyze the surface pressure and the important parameters controlling attenuation.

III. Results and Discussion

This section provides a detailed study of unsteady surface pressure measurements for the different canopy configurations shown in Table 1. The goal here is to understand how canopies alter the measured pressure spectra when placed over surfaces. The characteristics of reduction in the surface pressure can then be used to manipulate different regions of the boundary layer to obtain optimum noise reduction. This is done by firstly obtaining and analyzing the attenuation spectra. Second, the effect of the canopy geometric parameters such as the height, h, streamwise distance, x, rod diameter, d and spacing, S on attenuation is analyzed. Finally, the effect of the canopy on spatial and temporal characteristics of surface pressure correlations are examined.

A. Surface Pressure Measurements - Clean wall (untreated) Configuration

The untreated configuration corresponds to the undisturbed wall jet boundary layer flow without canopies. Surface pressure spectra obtained from this serves as the reference against which spectra for all the canopies are compared. Surface pressure measurements for the untreated case were made at four different jet speeds ranging 20 – 50 m/s in steps of 10 m/s. These measurements were performed using Knowles (FG-23329-P07) microphones placed at the canopy leading edge location, 1.13 m from the nozzle exit, shown in the previous section. The spectral data at frequencies less than 90 Hz has been neglected since it lies below the microphone response limit and the cut-off frequency of the facility. The higher limit of the microphone frequency range is ≈ 10 kHz .

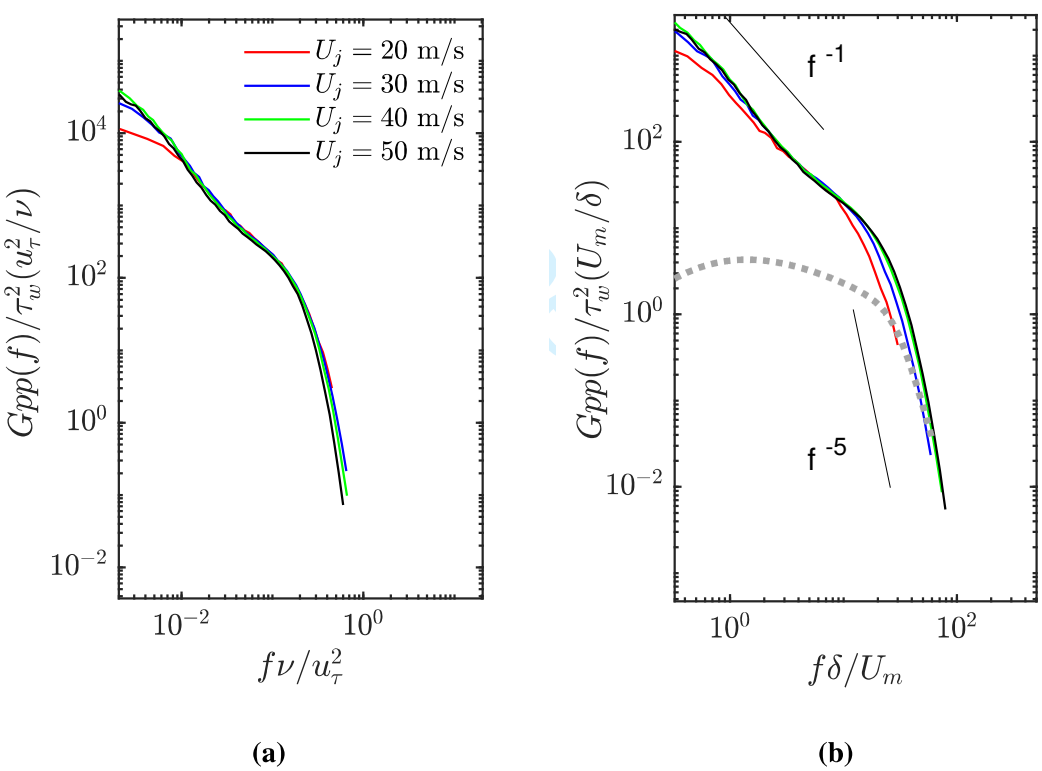

Fig. 6 Surface pressure spectra for the wall jet boundary layer scaled using a) inner and b) outer boundary layer variables [48]. The runs correspond to jet speeds 20-50 m/s. The dotted grey curve is the surface pressure spectra prediction using Goody model[54]

Figure 6 shows the untreated surface pressure spectra scaled on inner and outer boundary layer variables. The mean flow variables are obtained using algebraic equations by Wygnanski et al. [1] for the wall jet based on mean velocity measurements, details of which are provided in Kleinfelter et al. [44]. Outer scaling variables, boundary layer thickness, δ, boundary layer velocity, U_m and wall shear stress, τ_w [55] scale the low frequency spectra, $f\delta/U_m$ up to 10 [48]. The high intensity spectral fluctuations in the low frequency range are caused by the large, highly energetic turbulent eddies. The f^{-1} scaling in the log region and f^{-5} scaling at higher frequencies suggested by Blake [56] for a conventional turbulent boundary layer flows are compared with the wall jet spectra shown

in Figure 6b). The wall jet spectra has an additional low frequency region compared to canonical boundary layer due to the presence of an outer mixing layer in the boundary layer. Highly energetic turbulent interactions associated with the outer region cause the deviation of the wall jet pressure spectrum from the conventional surface spectrum at frequencies below $f\delta/U_m$ of 0.01, see Fig 6a). The high frequency spectra at non-dimensional frequency, $f\nu/u_\tau^2 > 0.1$ collapse using inner variables which are the viscous time-scale, ν/u_τ^2, friction velocity, u_τ and the wall shear stress, τ_w. Studies by Gersten [41] and Katz et al. [43] observed that inner wall jet boundary layer characteristics was similar to that of the flat plate zero-gradient turbulent boundary layer. At every streamwise location, measurements are performed for baseline(untreated or clean-wall configuration) and with (treated) the canopy. The skin friction velocity, u_τ as mentioned before has been estimated using the empirical relation given by George et al. [42].

B. Surface Pressure Measurements - Canopy

Canopies when placed in the turbulent wall jet boundary layer exhibit broadband attenuation in the unsteady wall pressure fluctuations. Figure 7a) compares a representative case of wall pressure spectra for canopy A placed at height, h of 6 mm($h/\delta = 0.4$) at a streamwise distance x =101.4 mm and jet velocities U_j, 20 to 50 m/s. This canopy most closely resembles the unidirectional, fiber canopies tested by Clark et al. [29] but without the leading edge support structure. It also mimics the open-area ratio of ~70% found in the owl's downy coating [47]. The absence of a leading edge support allows us to inspect the canopy flow independent of any additional upstream disturbances. Figure 7c) shows the attenuation spectra of Canopy A as a function of frequency at U_j ranging from 20 m/s to 50 m/s. The attenuation is observed over two frequency ranges: low frequency region (< 1 kHz) and high frequency range (> 1 kHz). The attenuation in the low frequency range increases with frequency until ≈4 dB and then drops marginally. Beyond 1 kHz, the attenuation is continuous and monotonously increases with frequency. The difference in the attenuation shift with speed in the two ranges indicate the possibility of two distinct pressure shielding mechanisms. Figure 7 c) shows that the low frequency peak attenuation appears to be independent of the flow speed for a constant canopy height. We observe a similar trend in surface pressure reductions for all the canopies tested.

The attenuation spectrum is computed as the difference between the measured pressure spectrum of the untreated , G_{pp_b} and canopy cases, G_{pp_c} and it is given by,

$$10\log_{10}(G_{pp_b}/G_{pp_c}) \tag{7}$$

Attempting to scale the attenuation spectra in the two regions, we find that in the lower frequency range, attenuation is invariant when plotted as a function of frequency normalized on the canopy height, h and the maximum boundary layer velocity, U_m, obtained from the PIV measurements [51, 52] at the canopy leading-edge location. Here, canopy A and canopy D, both with OAR of 66% have been shown as representative cases for the purpose of clarity. These canopies at h = 6 mm produce maximum, broadband attenuation clearly showing significant features of the surface pressure attenuation spectra. Subsequent sections show the results for all canopy configurations tested. Figure 8a) shows the attenuation spectra plotted with scaled frequencies for canopies A (d = 1 mm, s = 3 mm) and D (d = 2 mm, s = 6 mm) at h = 6 mm. A good collapse is observed until fh/U_m ≈0.2 where the attenuation has a maximum. This frequency range corresponds to convective

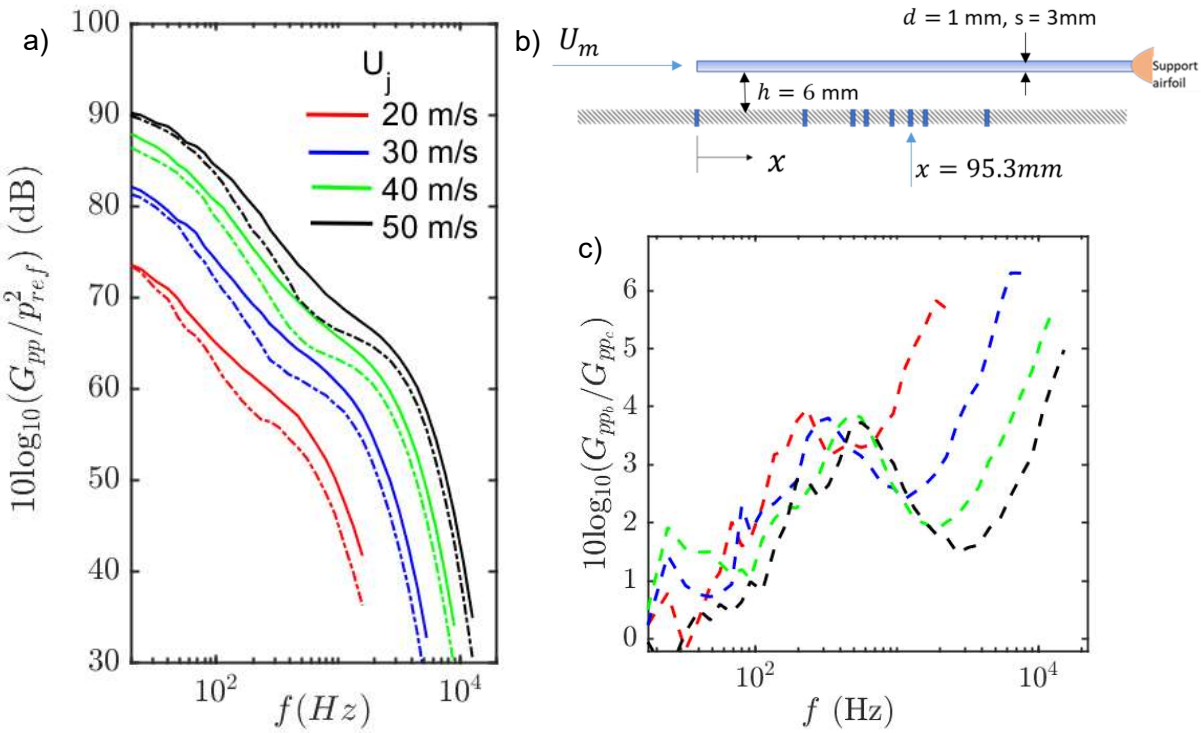

Fig. 7 a) Representative surface pressure spectra of Canopy A (dashed) compared with untreated configuration (solid) for four jet speeds. b) Schematic of canopy placement at canopy height, $h = 6$ mm and $x = 95.3$ mm ($x/h = 16$), corresponding to the measurement case shown c) Attenuation spectra for Canopy A at four jet speeds

scales much greater than the canopy height. Szoke et al. [51] suggest that the canopy acts as blockage thereby displacing the incoming flow in the wall-normal direction. This is hypothesized to generate a shearing effect perhaps resulting in stretching and breaking down of the larger, energetic turbulent eddies. The dominant timescale in this lower frequency range is associated with instabilities generated at the canopy height and propagating at mean flow speed.

Based on a conventional dissipative scaling, Fig 8b) shows the attenuation spectra for canopies A ($d = 1$ mm, $s = 3$ mm) and D ($d = 2$ mm, $s = 6$ mm) plotted against frequency normalized by ν/U_τ^2, where ν is the kinematic viscosity and U_τ is the friction velocity obtained at the canopy leading-edge using wall jet relations given by George et al. [42]. The high frequency scaling of the attenuation spectra is hypothesized to be associated with the viscous action slowing down the flow in the region below the canopy. Szoke et al. [51] show a reduction in the skin-friction velocity at the wall obtained both experimentally and computationally due to deceleration of the mean flow below the canopy. The high frequency scaling however does not collapse the attenuation magnitude between different canopies, indicating a suitable magnitude scaling is required accounting for the geometric parameters. For this reason, we will focus on plotting the attenuation using frequency

scaled on U_m/h. The dip in the attenuation observed in Fig 8 a) at fh/U_m, 0.2-1 is associated with increased turbulence generated at the canopy height. Nurani Hari et al. [52] show that attenuation in this regions observed a Strouhal number scaling based both on rod diameter and spacing.

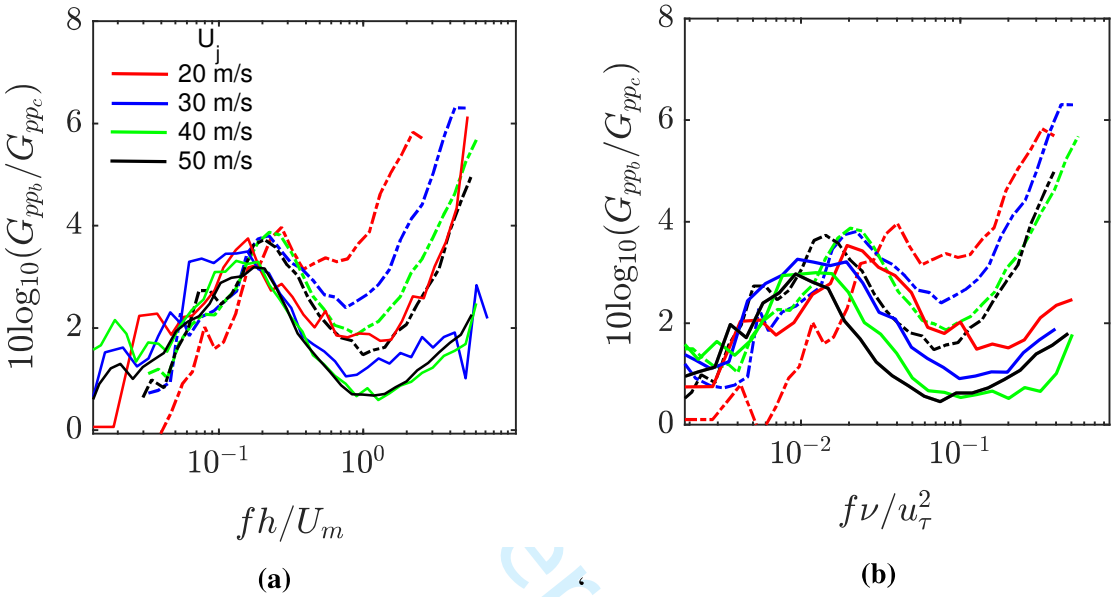

Fig. 8 Attenuation spectra, $10\log_{10}(G_{\mathbf{pp}_b}/G_{\mathbf{pp}_c})$ for Canopy A (dashed) and Canopy D (solid) plotted as a function of scaled attenuation, a) fh/U_m (low frequency scaling) b) $f\nu/u_\tau^2$ (high-frequency scaling)

Figure 9 shows the surface pressure spectra measured at different spanwise locations (Figure 3) for canopy D at height of 6 mm are nearly similar within the uncertainty limits. Further, prior tests conducted as a part of this study suggest that the measurements made by microphones placed in the gap between two adjacent rods and microphones below the rods showed similar magnitudes and trends in surface pressure attenuation. We expect discrepancy near the spanwise edges of the canopy however, in the present work, surface pressure measurements have been made with microphones placed in the gap between rods up to 75% of the entire canopy span.

1. Effect of streamwise scales

Figure 10 shows the attenuation spectra for canopies A-F at varying x/h and jet velocity, U_j of 50 m/s. The streamwise distance from the leading edge of the canopy can change the flow field and the corresponding surface pressure fluctuation characteristics. To understand better, the effect of x/h has been tested by varying canopy heights, h and streamwise distance, x individually. This ratio from previous studies on the canopy is indicated as an important parameter effecting surface pressure reduction [38]. We obtain a trend that is consistent for all canopies tested at varying jet speeds. The resulting attenuation spectra are plotted as a function of the normalized frequency, fh/U_m to gain better insights about the low frequency attenuation characteristics. Surface pressure measurements in Fig 10 have been shown for microphone locations from 50.5 mm (Mic 2) to 101.6

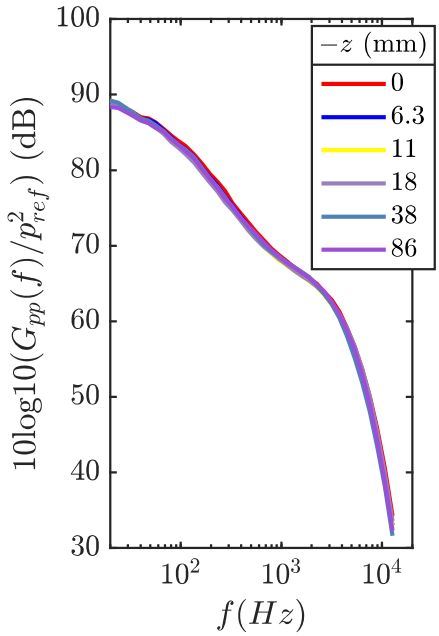

Fig. 9 Surface pressure spectra of the wall jet boundary layer for canopy A placed at height, $h = 6$ mm and $U_j = 50$ m/s measured at different spanwise locations

mm (Mic 7) beneath the canopy (see Fig 3 for mic locations). Figure 10 shows two sets of data, one corresponding to varying heights, $h = 6, 8, 12$ mm keeping x fixed at 101.6 mm and second, varying x for a fixed height, h of 6 mm. For canopy A, additionally, attenuation is presented for canopy heights, h of 2 mm, 4 mm and 15 mm to show the effect of the entire inner boundary layer region of the wall jet with δ of 15 mm at U_j of 50 m/s.

The results for increasing canopy height at a streamwise location in Fig 10 for all canopies shows a consistent reduction in attenuation levels. Studies conducted on finlets by Afshari et al. [34] indicate formation of a shear layer at the finlet height, which seem to be responsible for low frequency attenuation. For the current study, mean flow profiles below and above the canopy indicate a possible generation of a shear layer at the canopy height due to local friction exerted by the rods. The inflection in the mean velocity profile at the canopy height shifts away from the wall with increasing canopy height thus reducing the effect on the wall pressure. Jimenez et al. [37] also specifically studied the effect of introducing an inflection profile to a conventional boundary layer resulting in a mean profile similar to that of the canopy and showed suppression in the low frequency surface pressure. The reduction in the larger structures responsible for low frequency, high intensity surface pressure fluctuations scales with fh/U_m which justifies the collapse in low frequency canopy attenuation spectra.

In the case of Canopy A, h of 2 mm follows a different trend with a monotonous increase in attenuation with frequency. The absence of the low frequency attenuation below fh/U_m of 0.1 indicates that the canopy A at 2 mm acts to increase the wall-friction and the dissipation rate which effect higher frequencies. Beyond $h = 4$ mm, low frequency attenuation for all canopies show a collapse with fh/U_m up to the peak attenuation at $fh/U_m = 0.02$. At $h = 15$ mm, the canopy is placed nearly at the boundary height and produces lowest attenuation. Even though there is deficit

created in the mean profile even at larger height, the effect does not propagate to the wall, therefore we do not observe a reduction in the broadband attenuation levels. A similar trend for all canopy configuration is observed for the three canopy heights demonstrated in Fig 10 except for Canopy F, which has a negligible effect on low frequency attenuation. The effect of open-area ratio will be discussed in the following section.

Figure 10 also shows the effect of increasing streamwise distance from the canopy leading edge on the surface pressure attenuation. Flow analysis performed using wall-normal PIV showed that the streamwise development of the flow between the canopy and wall has a strong influence on the broadband attenuation levels [51]. The results for increasing the streamwise distance for instance in Fig 10a) while keeping the canopy height fixed show only slight increase in the attenuation particularly at high frequencies, fh/U_m above 1. For all canopies shown in Fig 10, we observe that the most upstream position has a significantly lower attenuation compared to other streamwise locations. Beyond x/h of 12, for example in Fig 10a), the attenuation spectra nearly collapse on each other within the uncertainty indicating that attenuation becomes invariant with further increase in x. Observing variation in the x/h ratios for Canopy A, the attenuation at low frequencies, fh/U_m <0.02 seems to be invariant beyond $x/h \approx 15$. Szoke et al. [51] show evidence that low frequency attenuation saturate once the turbulent boundary layer generated over the rods starts to interact with the wall, which occurs at $x/h \sim 15$. To better understand the relation of the attenuation growth rate and magnitude with x/h, we trace the peak attenuation value at $fh/U_m = 0.02$ for all test cases.

Figure 11 shows peak low frequency attenuation values measured at $fh/U_m = 0.02$ for all canopies as a function of x/h. At lower x/h values associated with development region of the boundary layer around the rods, the peak low frequency attenuation continues to increase with x/h. The rate of attenuation has a slope which appears to depend on the canopy open-area ratio. For canopies A, B and D with the same OAR of 66%, the slopes given by the dotted black line is ≈ 0.25. E has a slightly slower attenuation growth rate with x/h even though it has the same OAR. With an increased OAR to 75% and 88% for canopies C and F respectively, the streamwise growth of the peak attenuation attained reduces. Also for canopies A and B, there is a distinct region at $x/h > 15$, where the attenuation saturates and becomes invariant with further increase in x/h.

2. *Effects of Canopy geometry*

This section focuses on understanding the effect of canopy geometry on the surface pressure attenuation. The open-area ratio (OAR) is the measure of area that allows vertical transfer of flow quantities and is similar to porosity. As we increase the OAR, the flow tends to become similar to the untreated configuration. We tested three OAR configurations, 66%, 75% and 88% with same rod diameter of 1 mm. Figure 12 a) shows the attenuation spectra plotted with fh/U_m for canopies A, B, D and E with the same OAR of 66% and 12 b) compares the attenuation spectra for Canopies A, C and F with varying OAR of 66%, 75% and 88% respectively. All the data shown here correspond to $h = 6mm$, $x = 101.6$ mm and U_j of 50 m/s.

For the same OAR, the low frequency attenuation is nearly invariant. There is however a reduction in the peak magnitude of attenuation with increase in rod diameter for the same OAR canopies. The results in Fig 12 b) show that the broadband attenuation magnitude reduces with

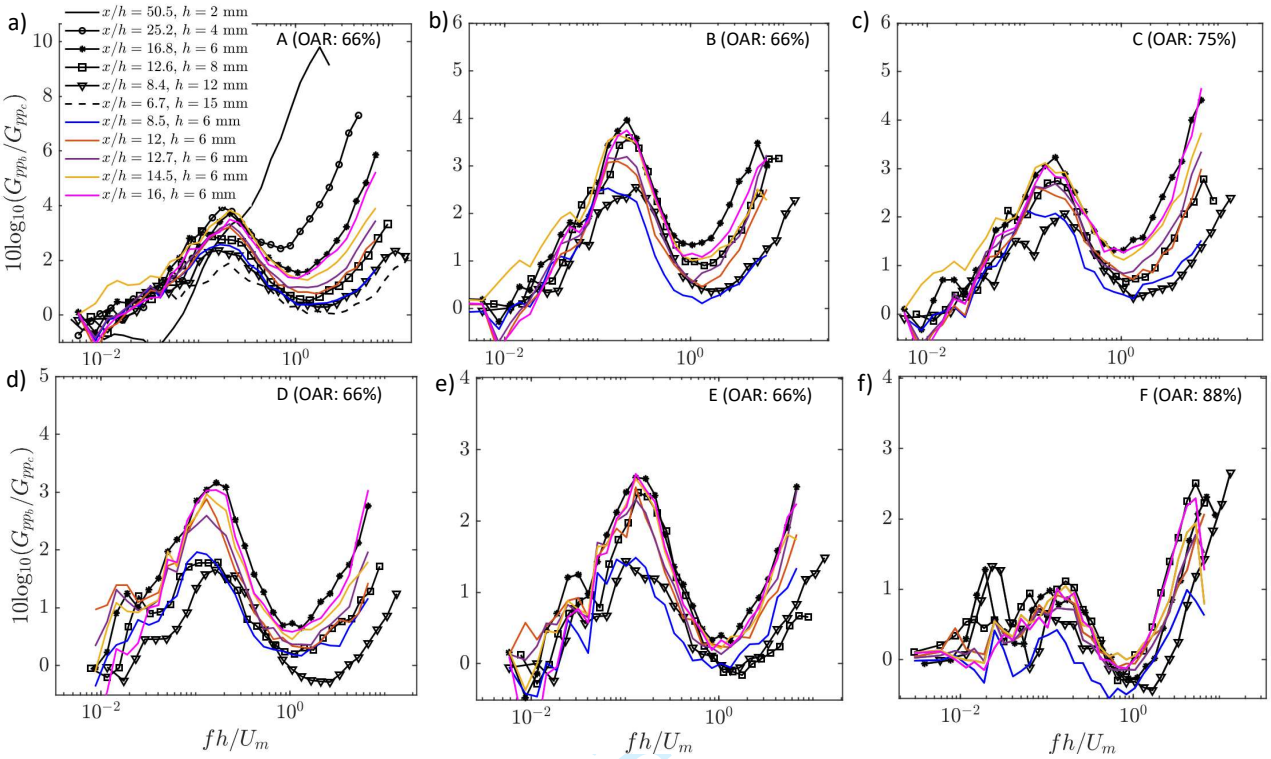

Fig. 10 Attenuation spectra for canopies (a) A (d = 1 mm, s = 3 mm), (b) B (d = 1.56 mm, s = 4.68 mm), (c) C (d = 1 mm, s = 4 mm), (d) D (d = 2 mm, s = 6 mm), (e) E (d = 3 mm, s = 9 mm) and (f) F (d = 1 mm, s = 8 mm) plotted against scaled frequency, fh/U_m at varying ratio of streamwise distance and canopy height, x/h at U_j of 50 m/s

increasing open-area ratio. The mean velocity deficit [38, 51] created by the canopy is dependent on the leading edge blockage and shear generated over the canopy rods. For the same diameter, as the OAR increases, the relative wetted area reduces resulting in a lower shear strength. Such a configuration can allow more vertical velocity momentum transfer across the canopy retaining a largely undisturbed flow. Smaller open-area ratio (Canopy A, Fig 12 b) possibly obstructs and dampens the wall normal velocity in the region between the wall and the canopy, therefore resulting in a lower surface pressure amplitude. The low frequency spectra for Canopies A (66%) and Canopy C (75%) are nearly the same since the spacing for the two cases are 3 mm and 4 mm respectively therefore, it is possible that the shear layer generated over the two canopies has nearly the same strength. Canopy F (88%) shows a significant reduction in attenuation indicating that increased OAR reduces the broadband attenuation. At low frequencies attenuation depends on ratio of streamwise distance over canopy height, x/h, strouhal number, fh/U_m and the open-area ratio, $S/(S+d)$. As seen before, x/h is indicative of readjustment of the boundary layer due to the presence of the canopy while $S/(S+d)$ controls the growth rate and magnitude of attenuation with x/h. Attenuation at higher frequencies however is not a unique function of either of the parameters.

The surface pressure attenuation by canopies as we saw in section II.E can depend on a number of parameters. In order to design an optimized canopy, we can first start with understanding the

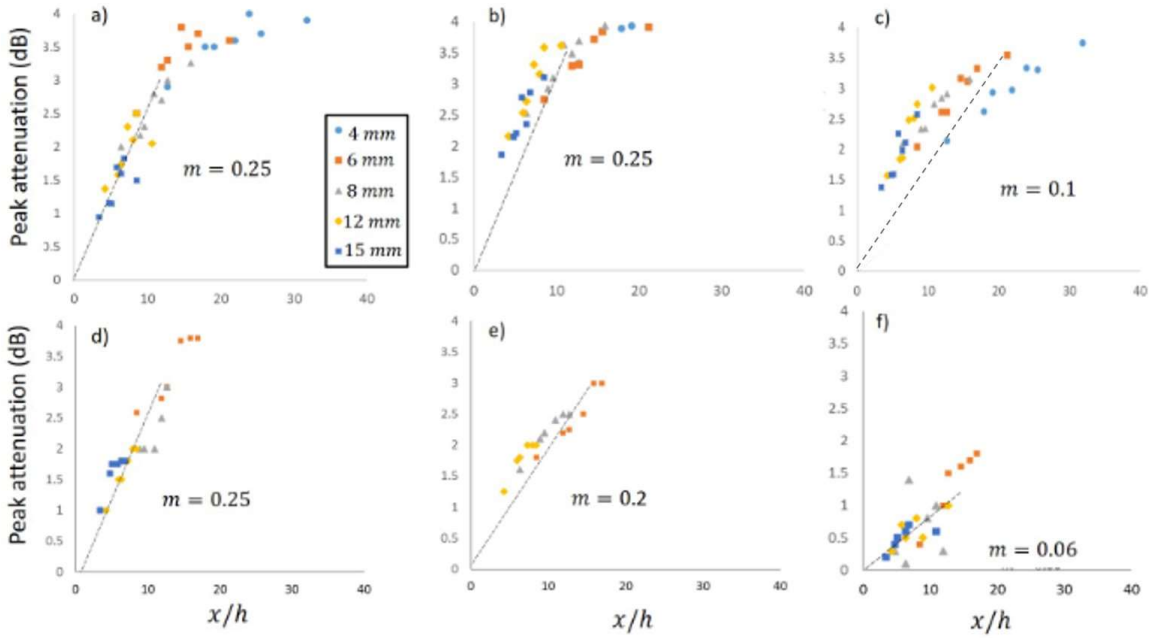

Fig. 11 Low frequency peak attenuation plotted as a function of the streamwise distance normalized on the canopy height, x/h for canopies (a) A (d = 1 mm, s = 3 mm), (b) B (d = 1.56 mm, s = 4.68 mm), (c) C (d = 1 mm, s = 4 mm), (d) D (d = 2 mm, s = 6 mm), (e) E (d = 3 mm, s = 9 mm) and (f) F (d = 1 mm, s = 8 mm). Straight lines from the origin indicate average slope (m) of the developing attenuation region.

placement of the canopy with respect to the boundary layer. So first, from all the test cases, we find the optimum range of h/δ ratio. Figure 13a) shows the attenuation spectra for all canopies A-F, placed at different heights in the boundary layer at a reference jet velocity, U_j of 50 m/s. Each colour represents the height and the markers indicate different canopy configurations as shown in the legend on Fig 13a). There is a broadband increase in attenuation spectral magnitude with reducing h/δ. For values less than $h/\delta \leq 0.4$, the low frequency attenuation nearly saturates and becomes invariant. The attenuation spectra is much lower for h/δ values greater than 0.4 so the optimum value could be chosen to be 0.4. From Fig 10 a), we know that if the canopy is placed very close to the wall, $h \leq 2$ mm ($h/\delta \leq 0.13$), the low frequency attenuation is nearly zero. Therefore, the ideal choice of h/δ would range between 0.25-0.4. Since the attenuation at lower frequencies scales with fh/U_m, the effective frequency range can be obtained for any canopy height given the flow speed. Next, if we were to decide on the canopy rod diameter, Fig 13b) shows the attenuation as a function of rod diameter for canopies A, B, D and E at a height, h = 6 mm as an example. There are two regions of attenuation observed, both of which are significant at $d/h < 0.3$. Therefore, maximum rod diameter for effective attenuation would be $0.3h$. The absence of attenuation at mid-frequencies ranging $0.6 < fh/U_m < 2$ shows the canopies produce turbulent self-noise for all canopy diameters which reduces the surface pressure attenuation. This is substantiated by mid-frequency attenuation scaling, fd/U_m proposed by Nurani Hari et al. [38]. Similarly, if we look at the attenuation contour

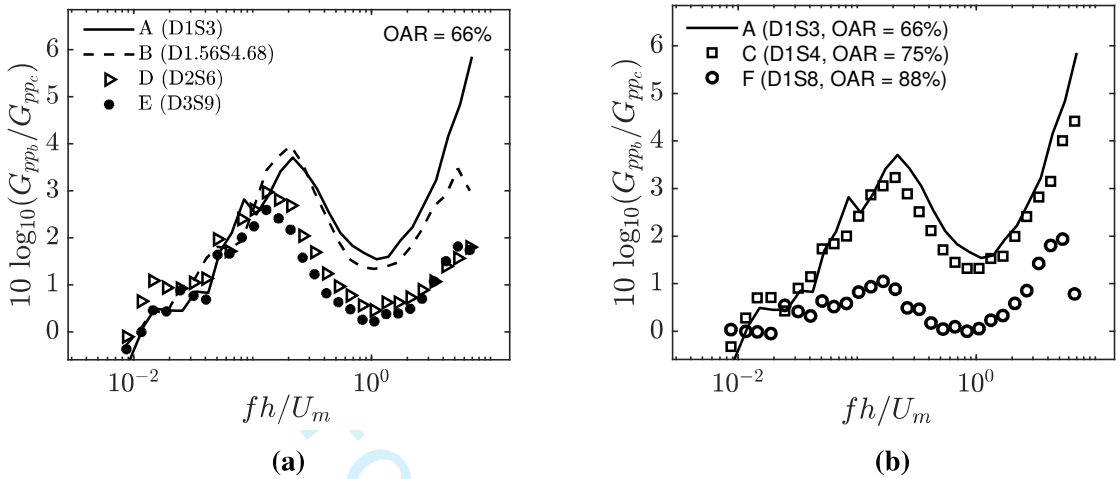

Fig. 12 a) Attenuation spectra plotted against scaled frequency, fh/U_m for canopies A, B, D, E with the same open-area ratio, measured at x =101.4 mm (x/h = 16.8) b) Attenuation spectra plotted against scaled frequency, fh/U_m for canopies A, C and F with varying open-area ratio, measured at x =101.4 mm (x/h = 16.8) and U_j = 50 m/s

as a function of s/h in Fig 13c), we observe significant attenuation in the lower and higher frequency ranges for values of $s < 0.6h$. These optimized design parameters could now be used to build canopies for different aerodynamic applications.

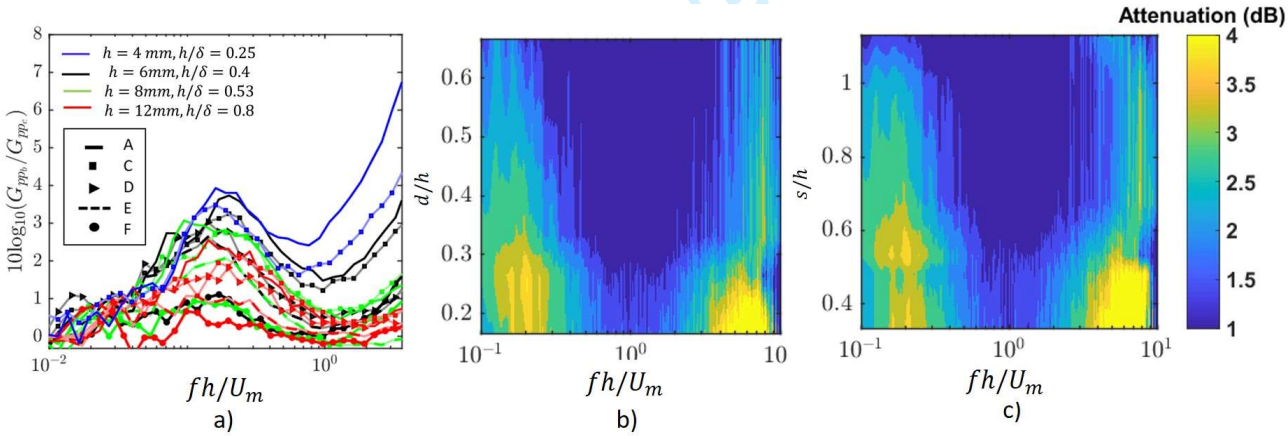

Fig. 13 a) Attenuation spectra plotted against fh/U_m for canopies A-F at h =4, 6, 8 and 12 mm, U_j of 50 m/s, measured at x =101.4 mm (x/h = 16.8), b) Attenuation contourmap as a function of varying ratios of diameter over canopy height, d/h and scaled frequency, fh/U_m c) Attenuation contourmap as a function of varying ratios of spacing over canopy height, s/h and scaled frequency, fh/U_m

3. Effect of entrance condition

The canopy can be rotated about the airfoil support and we can tilt it such that the leading edge touches the wall to generate an entrance condition. Figure 14 shows a representative case of tilted canopy A at angles 2.4 degrees and 4.8 degrees. The results can be compared to the attenuation spectra of parallel canopy A configuration shown in Fig 7c). Two main observations can be made here in Fig 14a). Firstly, there is a significant difference in the attenuation spectrum obtained for angled canopy compared to parallel orientation. Secondly, introducing an entrance condition has a broadband effect where the lower attenuation is suppressed while the high frequency attenuation is enhanced. Attenuation curves look strikingly similar to those obtained by Clark et al. [47]. Surface pressure reduction in tilted canopies are dominated by dissipative mechanism than the shear-generation mechanism. This could be due to reduction in length scales caused by presence of solid canopy elements extending from the wall therefore producing smaller scale structures not only at a particular height but at range of heights. Overall, we found that the leading edge condition enhanced the surface pressure attenuation in the higher frequencies. The lower frequency attenuation is observed to be slightly suppressed showing a monotonic increase in attenuation with frequency. However, when we increase the leading edge angle (Fig 14b), measurement at the same location shows that the attenuation starts developing into two distinct frequency regions as seen in parallel canopies, presumably associated with inviscid mechanisms at low frequencies, and viscous dissipation at high frequencies. We conclude that the canopy entrance condition is an important component of the surface pressure attenuation.

C. Temporal and spatial characteristics

This section talks about the cross-spectral characteristics of surface pressure measurements which helps us in understanding the propagation of the unsteady pressure in the space-time domain. This has been done by analyzing the streamwise and spanwise coherence of the surface microphone data. The space-time correlations for the untreated and canopy cases are compared and effect on the broadband convection velocity is analyzed.

1. Streamwise Coherence

Streamwise coherence, γ^2 gives us the spatial extent of the pressure fluctuations in the flow direction. Figure 15 shows the streamwise coherence contour for the clean-wall configuration (left-most figure) and canopy D (center figure) at jet speed of 50m/s for separation distances, Δx ranging from 4 mm to 127 mm (see Figure 3, for microphone array). The contour level spacing corresponds to the maximum uncertainty in the coherence value of 0.02. The contour plots of the wall jet boundary layer show similar pattern as observed in a conventional turbulent boundary layer, with a wider spread at lower frequencies and gradually diminishes to a thin region at the higher frequencies. This indicates that the eddies are strongly correlated at smaller streamwise separations. At low frequencies, the streamwise coherence remains significant even at larger separations exhibiting that larger eddies persist over longer streamwise distances. The eddies are thus highly coherent at smaller distances but gradually become less coherent as they convect to larger separations. As we move to higher frequencies, the coherence levels remain prominent only

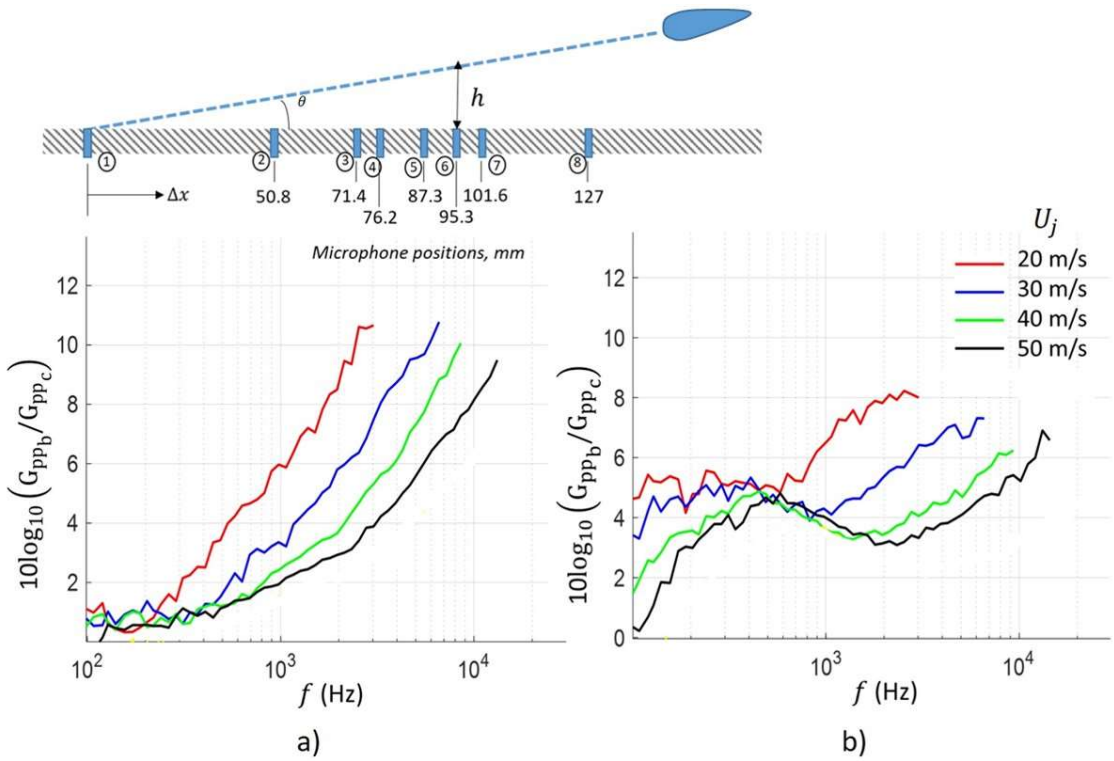

Fig. 14 Tilted canopy attenuation as a function of frequency (Hz) for canopy A at a) 2.4 degrees and b) 4.8 degrees measured at $x/h = 23.9$

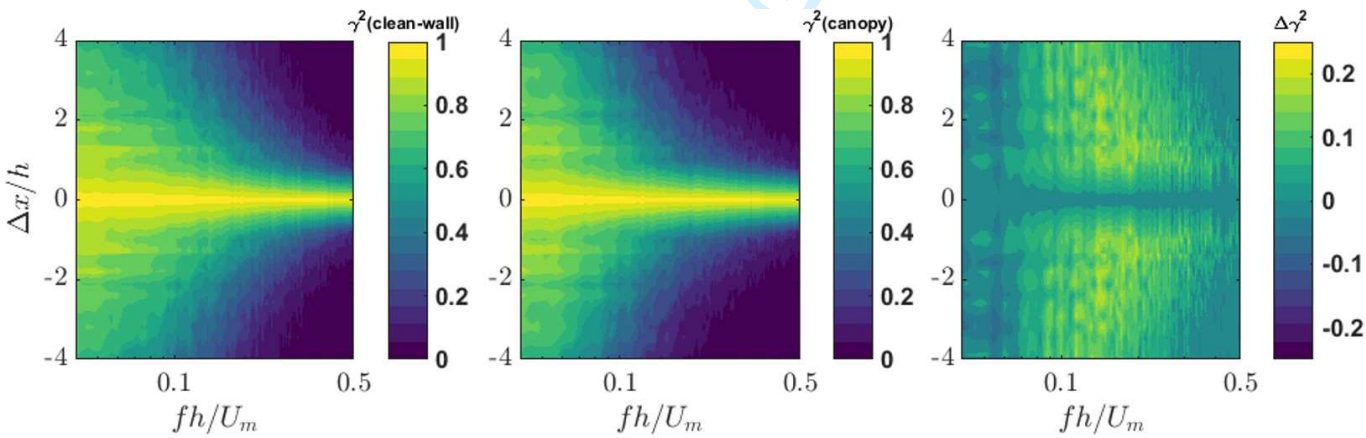

Fig. 15 Streamwise coherence, γ^2 of surface pressure fluctuations as a function of scaled frequency, fh/U_m and normalized streamwise separation, $\Delta x/h$ for (LEFT) clean-wall configuration and (CENTER) canopy D ($d = 2$ mm, $s = 6$ mm) at $h = 6$ mm and $U_j = 50$ m/s. (RIGHT) Difference in the coherence levels of the clean-wall and canopy configurations, $\Delta\gamma^2 = \gamma^2_{clean-wall} - \gamma^2_{canopy}$

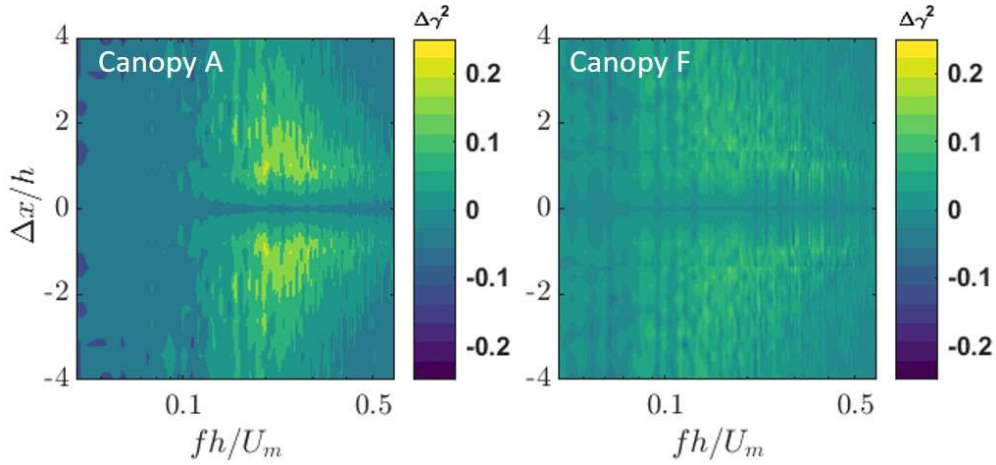

Fig. 16 $\Delta\gamma^2$ as a function of the normalized frequency, fh/U_m and separation, $\Delta x/h$ for canopy A (OAR=66%) and F (OAR=88%). The baseline used is the same as the clean-wall configuration shown above in Figure 15

at smaller separation distances, thus indicating that the smaller structures rapidly loose coherence with increasing separation. The $\Delta\gamma^2$, calculated as, $\gamma^2_{clean-wall} - \gamma^2_{canopy}$, shows that the canopy reduces the streamwise coherence at frequencies ranging between, fh/U_m 0.1-0.6 (right-most, Figure 15). This frequency range corresponds to reduction in the large and mid-scale structures which are associated with the outer mixing layer region [48]. Reduction in coherence is observed for streamwise separations up to $\approx 4h$ which indicates a reduction in these large-scale, energetic eddies that are responsible for the low-frequency surface pressure spectra. Figure 16 shows the change in streamwise coherence, $\Delta\gamma^2$ for canopies A and F at jet speed of 50 m/s and height, h of 6 mm. Canopy A (OAR = 66%) shows a lower reduction in the coherence compared to canopy D (OAR = 66%) even though it shows higher attenuation spectral levels. This establishes that the increased rod spacing affects the attenuation in the surface pressure while the rod diameter has a greater effect on the streamwise cross-correlation characteristics of surface pressure. Canopy F (d = 1 mm, s = 8 mm) with the highest open-area ratio of 88% seems to have the least effect on the streamwise coherence.

2. Spanwise Coherence

The spanwise extent of turbulent structures is an important factor along with the surface pressure spectra in generation of trailing edge noise [57]. To understand the impact of canopies on the spanwise distribution of turbulence, the spanwise coherence and the spanwise turbulent integral length scale is now investigated. Figure 17 shows the spanwise coherence as a function of the spanwise separation and frequency, for Canopy D (middle image) compared with the clean wall configuration (left image) at U_j of 50 m/s. The maximum uncertainty in the spanwise coherence is 0.02. The coherence along the span is narrower than the streamwise coherence and extends only up to spanwise distances of $2h$ at lower frequencies, fh/U_m of 0.1. Coherence beyond fh/U_m of 0.2 quickly drops indicating only large fluctuations persist at larger spanwise distances. The spanwise

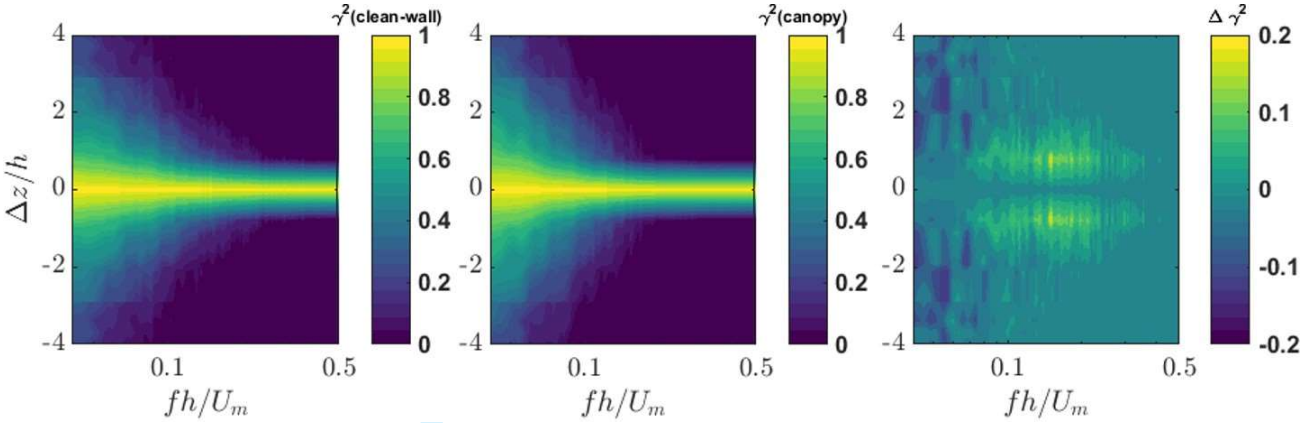

Fig. 17 Spanwise coherence contour maps of surface pressure fluctuations as a function of fh/U_m and $\Delta z/h$ comparing the clean-wall and canopy D (d = 2 mm, s = 6 mm) at h = 6 mm for U_j of 50 m/s. The left most column is the coherence contour for clean-wall case, $\gamma^2_{clean-wall}$, center column is the γ^2_{canopy} for canopy D and rightmost column is $\Delta\gamma^2 = \gamma^2_{clean-wall} - \gamma^2_{canopy}$

array is located 76.2 mm downstream from the canopy leading edge, therefore the attenuation may not be fully developed here, however it is helpful to understand how the canopy alters the spanwise turbulence lengthscale. We can expect these effects to be more profound as we go further downstream to fully developed attenuation region. For microphones separations of more than $2h$, the coherence drops to less than 0.4. $\Delta\gamma^2$ measured as the difference between clean-wall and canopy configurations shows a reduction in spanwise coherence at fh/U_m ranging 0.08 - 0.4. This is in agreement with the lower frequency range of the surface pressure attenuation showing breaking down of larger turbulent eddies by the canopies along the span. The coherence colormaps show that the pressure fluctuations remain largely uniform in the spanwise direction below the canopy. There is a slight increase in the spanwise coherence observed at $fh/U_m < 0.08$. Figure 18 shows $\Delta\gamma^2$ for canopy D for heights 8 mm, 12 mm and 15 mm for jet speed, U_j of 50 m/s. The magnitude of reduction in the spanwise coherence is more prominent for canopies closer to the wall. The collapse of the spanwise lengthscales on the canopy height confirms that h and U_m are significant in controlling low frequency attenuation.

The spanwise extent of the unsteady surface pressure coherence is an important parameter in the trailing edge noise generation to the far-field. Amiet [57] modeled the far-field noise source term on the product of the surface pressure fluctuations with its spanwise lengthscale. This can be computed as the integral of the spanwise coherence with respect to the spanwise microphones separations, given by

$$l_z(f) = \int_0^\infty \gamma_z^2 dz \tag{8}$$

Figure 19a) shows the spanwise lengthscale normalized on canopy height plotted as a function of fh/U_m. The lengthscale is larger at small values of the normalized frequency, fh/U_m indicating larger structures contribute towards low frequency coherence. There is a reduction in spanwise lengthscales observed with canopies in the frequency range, $0.04 < fh/U_m < 0.06$ at U_j of 20 m/s.

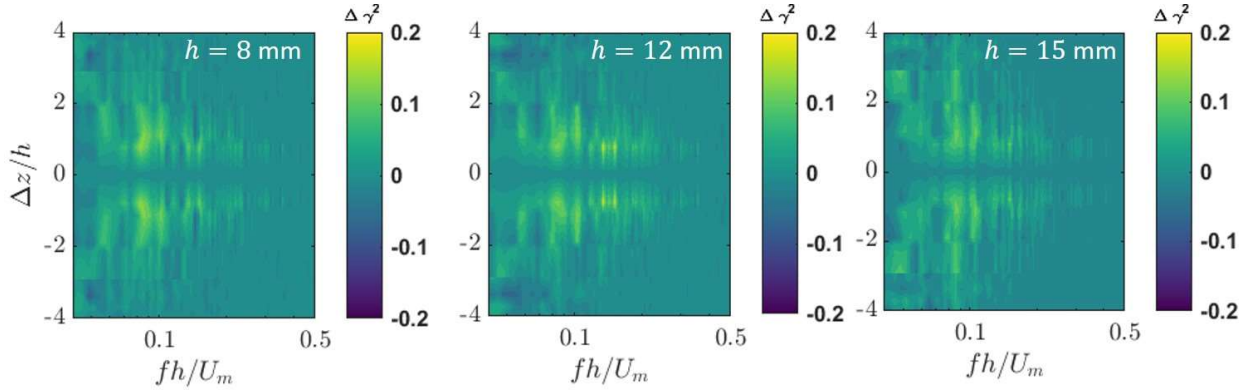

Fig. 18 Difference in the spanwise coherence, $\Delta\gamma^2 = \gamma^2_{clean-wall} - \gamma^2_{canopy}$ of surface pressure fluctuations for Canopy D (d = 2 mm, s = 6 mm) for different canopy heights, a) h = 8 mm b) 12 mm, c) 15 mm. The data corresponds to jet velocity of 50 m/s.

The effect on the spanwise lengthscale seems to be adverse at lower fh/U_m below 0.04 at 20 m/s, however, the difference in the magnitude reduces with increasing flow velocity. The normalized spanwise lengthscale collapses well for increasing canopy heights, indicating h is the dominating factor at low frequencies, as shown in Fig 19b).

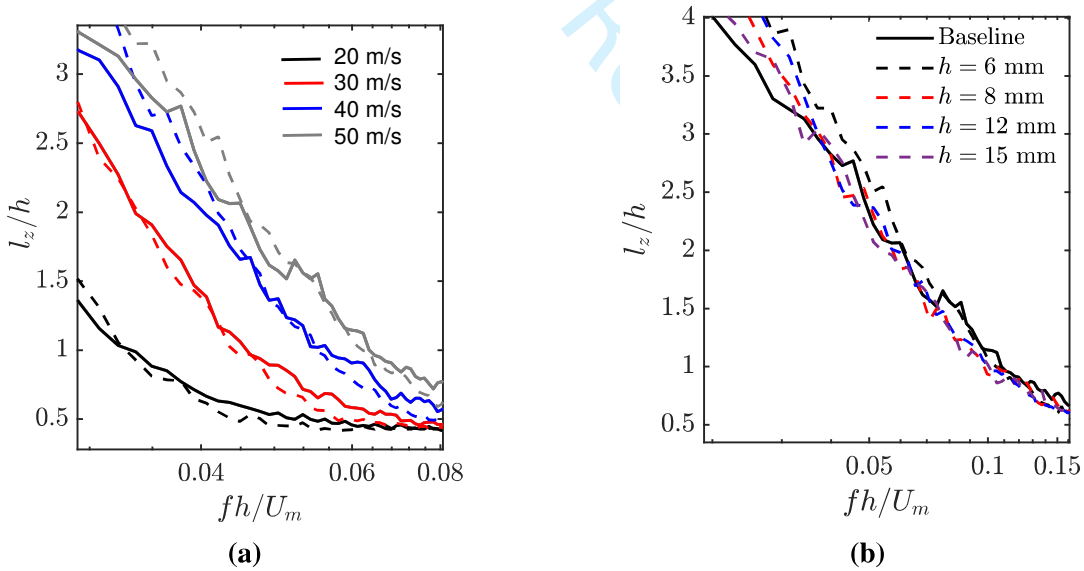

Fig. 19 Spanwise lengthscales of wall pressure correlations for untreated (solid) and canopy (dashed) configurations. Measurements show Canopy D (d = 2 mm, s = 6 mm) at height of 6 mm for U_j ranging from 20 m/s (red), 30 m/s (blue), 40 m/s (green) and 50 m/s (black) as a function of normalized frequency, fh/U_m

3. Space-time correlations

Evolution of wall pressure space-time correlation, R_{pp}, between the pressures measured at two streamwise location, x and $x + \Delta x$, and at t and $t + \Delta t$, in a homogeneous, stationary flow is given by,

$$R_{pp} = \frac{\overline{p'(x,t)p'(x+\Delta x, t+\Delta t)}}{\sqrt{\overline{p'^2}(x,0)}\sqrt{\overline{p'^2}(x+\Delta x,0)}} \tag{9}$$

Figure 20 (left-most) shows the streamwise correlation as a function of normalized streamwise separations, $\Delta x/h$ and time delay, $\tau U_m/h$ for the untreated case with flow at 50 m/s. The abscissa shows the time delay, τ, which is normalized on the ratio of boundary layer maximum velocity, U_m over canopy height, h. The streamwise separations, Δx on the ordinate axis are normalised by canopy height, h. The contour map shows the region of high correlations known as the convective ridge along the diagonal of the plot, with highest correlations near smaller streamwise separations and smaller time delays. Near the origin of the plot, where the time delays and the separations are small, the correlation is contributed by eddies of all sizes and therefore has the maximum value. With increase in streamwise separation and time delay, the correlation reduces. This is due to loss of energy of the smaller eddies which disintegrate rapidly with distance as they travel. The larger eddy structures associated with smaller frequencies prevail and tend to correlate well up to greater distances than the smaller eddies associated with higher frequencies. The slope of the correlation function is called the convective ridge and it symbolizes the streamwise extent of correlation with time. Near the origin, the eddies would have covered a very short distance in a short time remaining largely coherent. The variation in the slope of the convective ridge (dotted, black line, Fig 20) indicates that the associated turbulence convects at different speeds. The pressure convection velocity is often directly related to the flow speed and often assumed as a fraction of the same for analytical models [58][59]. At higher separations, the slope starts to reduce showing a reduction in the eddy speed, therefore taking a longer time to cover the same separation. The convective ridge slope starts to decrease beyond $\Delta x/h > 10h$ indicating that the eddies start moving slowly at higher separations away from the wall.

The correlation contour for the wall jet flow has a wider spread compared to a conventional boundary layer flow with the same boundary layer parameters [60]. This indicates higher time scales and therefore larger structures that extend beyond the boundary layer thickness. The most strongly correlated eddies with $R_{pp} > 0.6$ exist at small streamwise separations within $-5 < \Delta x/h < 5$ while the weakly correlated structures with $R_{pp} < 0.4$ persist over longer distances. The width of the contour slightly varies to show contributions from eddies of different sizes. The contour slightly thins down near smaller separations and time delays which indicates this region is largely influenced by smaller structures. The average width of the convective ridge is $\tau U_m/h \approx 10$. The contours of the space-time correlations seem to be oval shaped, with larger spread spatially than the temporal spread. This characteristic is also observed for canonical boundary layer flows where the correlation contours were oval shaped. There is a region of low correlation at higher streamwise separations, $\Delta x/h > 10$, observed in the wall jet due to decay in mean velocity in the outer region of the turbulent boundary layer. The correlation contours are observed to be symmetrical at smaller separations and time delays. With increase in separations, the correlations become stronger in the flow direction,

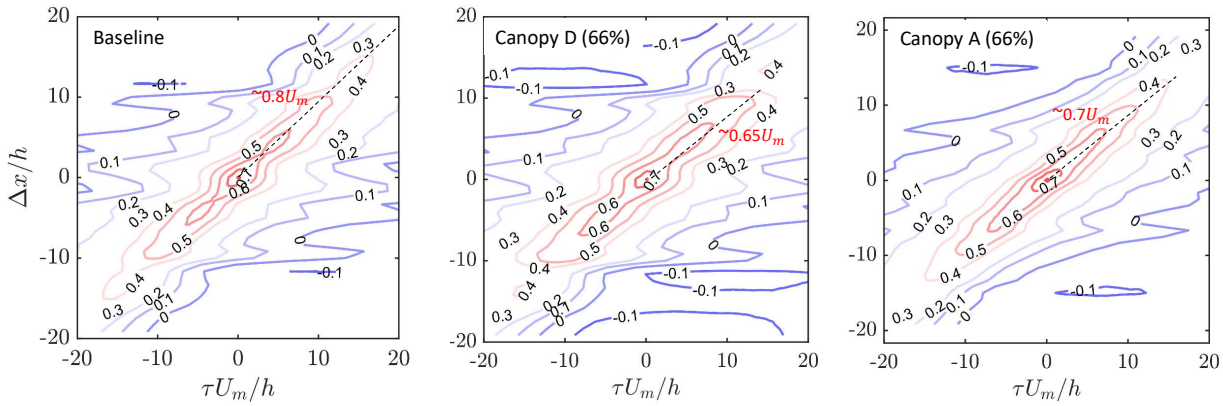

Fig. 20 Streamwise space-time correlation coefficient contour map, R_{pp} as a function of the normalized streamwise separations, $\Delta x/\delta$ with Δx ranging from 4 mm to 127 mm, and normalised time delay, $\tau U_m/\delta$ for (LEFT) clean-wall configuration (CENTER) canopy D at $h = 6$ mm (RIGHT) Canopy A at $h = 6$ mm

developing an asymmetry. At larger separations, the eddies become negatively correlated for smaller time delays.

For the canopy, the space-time correlations are similar to the untreated case. The width of the convective ridge is slightly wider for the canopy than that for the untreated wall therefore the spread of the correlation contour in the time delay axis seems to be higher for the canopy. The strong correlation region shown by the red contour is broader for the canopy indicating that correlation persists over slightly larger time delays for the same streamwise separations. This agrees with a slight increase in the mean velocity in the outer boundary layer region for canopies. Also note, the microphone arrangement for canopy A does not resolve separations ranging between $-1 < \Delta x/h < 1$. For both the canopies, the stronger correlations is observed at longer separations. The slope of the convective ridge increases at smaller separations and reduces at larger separations similar to the untreated case. The average slope of the convective region in canopy is lower than the slope observed in the untreated region. Similar to the untreated case, edges of the convective ridge at larger spatial separations reduces in slope indicating larger eddies away from the wall travel at a lower speed.

4. Convection velocity

The correlation function forms elongated contours along the diagonal which is referred as convective ridge, with a slope that changes with increase in streamwise separations and larger time delays as shown in Figure 20. The slope of the convective ridge indicates the convective velocity of the eddies as a function of the separation distances. The smaller separation distances have higher correlations, dominated by contributions coming from close to the wall. These eddies convect at lower velocities than the larger eddies which are further away from the wall. The bulk convection velocity is obtained by computing the slope along the convective ridge. The convection velocity of the eddies at very small streamwise separations increases. This is also observed for conventional

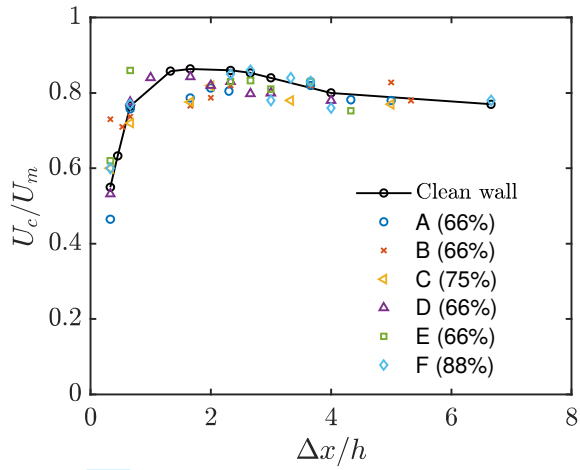

Fig. 21 Normalized pressure convection velocity as a function of the streamwise separations, $\Delta x/h$. The legend represents the canopy configurations from A to F

boundary layer flow. This comes out of the reasoning that the flow in the boundary layer increases from the wall to the boundary layer thickness height and therefore, the associated convective speed of the turbulence directly correlated with the unsteady pressure increases. The pressure convection velocity reaches a maximum and then starts to slow down with further increasing streamwise distance. This integrates well with our understanding of the distribution of turbulent sources contributing towards the unsteady wall pressure. The smaller eddies in the near wall dominate the smaller time delays and unsteady pressure at higher frequencies. The slower convective speeds at higher separations originate from the outer mixing layer. Figure 21 shows the comparison of the pressure convection velocities for the clean wall configuration and with canopies A-F at height, h = 6mm and jet speed of 50m/s. The convection speed for the canopies remains largely unaltered at smaller streamwise separations, $\Delta x/h < 2$. There is some reduction in the convection speeds observed for canopies A to E at separations ranging between, $2 < \Delta x/h < 4$, indicating there is perhaps some deceleration of the mean streamwise velocity around the canopy. However it is significantly close to the uncertainty value of 0.03 U_c/U_m. The plausible explanation for the reduction in the pressure convection velocity by the canopies is the reduction of the mean flow velocity around the canopies. The time-resolved PIV measurement [51] shows reduction in the mean flow below the canopy and generation of wake between the rods. The reduction in the mean velocity therefore causes the eddies to convect at slightly lower speeds. At larger distances, where we observe the pressure convection speeds to decay, there is no effect of the canopy. This indicates that the canopy does not alter the mean flow in the outer region of the mixing layer and thus the corresponding pressure convection velocities remains nearly the same.

IV. Conclusion

Experiments are performed on unidirectional, elemental canopy configurations, which are parallel arrays of streamwise rods that exhibit surface pressure reduction. The canopy height, rod

diameter and spacing are varied to study the effect of geometric parameters on the surface pressure. The streamwise and spanwise microphone array gives the spatial and temporal correlations of the surface pressure. The tests were run in the wall jet wind tunnel facility at Reynolds number, $U_m\delta/\mu$ of 6x10^3 - 12x10^3 measured at the canopy leading edge.

The surface pressure reduction can be characterized in two frequency regions. The low frequency, $fh/U_m < 0.2$ and high frequency, $fh/U_m > 1$ regions produce increase in the attenuation spectra with frequency. At mid frequencies, the reduction in attenuation attributed to new turbulence production. The low-frequency attenuation increases with distance downstream from the canopy leading edge $\Delta x/h$ when other parameters are held fixed and reduces with increase in open area ratio, canopy rod diameter and spacing. The rate at which the attenuation increases with x/h reduces with open area ratio. For a particular canopy at height h, the attenuation develops linearly with the streamwise distance up to x/h of 15-20, beyond which the attenuation saturates and becomes invariant with further increase in the streamwise distance. This is observed for all the canopies tested, therefore the low frequency attenuation appears to be a unique function of x/h. Placing the canopy closer to the wall increases the attenuation at higher frequencies. The peak magnitude of attenuation in the lower frequency range seems to depend on the open-area ratio, $S/(S+d)$ and ratio of rod diameter and canopy height, d/h. Surface pressure attenuation reduces with open-area ratio. The attenuation for the same open-area ratio shows a similar attenuation growth with x/h, indicated by slope of the attenuation curve. With increase in the open-area ratio, the growth in attenuation is slower and lower in magnitude. The two regions of attenuation indicate two separate scaling based on the flow physics. At low frequencies, attenuation collapses on a Strouhal number scaling given by frequency normalized by the canopy height, h and the maximum velocity in the boundary layer, U_m. The attenuation at high frequencies follows a dissipative scaling given by $f\nu/U_m^2$, where ν is the kinematic viscosity.

The spatial and temporal evolution of the unsteady pressure fluctuations in the wall jet reveals larger streamwise correlated structures extending to x of 0.1m or x/h of 16.67, where h is 6mm. The presence of the canopy shows reduction in the streamwise coherence at frequencies ranging between 0.3-1 kHz, indicating breakdown of large-scale fluctuations by the canopy. With decrease in canopy height, there is further reduction in the streamwise coherence from the untreated case. The spanwise extent of surface pressure show a marginal reduction due to the canopies at frequencies ranging 0.2-0.7 kHz. The two-point correlations of the wall jet unsteady surface pressure in the streamwise direction indicates slowing of the mean flow and loss in the energy of low frequency turbulence. This is also reflected in the reduction of pressure convection velocity at streamwise separation distances ranging 2-4h.

Canopies therefore reduce the intensity of the surface pressure when placed in a turbulent boundary layer. The effect on the cross-spectral quantities of the unsteady pressure appears to be less significant. Effective pressure shielding can be implemented by manipulating the geometric parameters of the canopy. Particle Image Velocimetry measurements of the flow around and beneath these canopies will elucidate the interaction of the rods with the flow-field. These can be further used to give insight on the dependencies observed in the wall pressure fluctuations.

Acknowledgement

The authors would like to thank the National Science Foundation, in particular Dr. Ron Joslin, for their support of this research under grant CBET-1802915.

References

[1] Wygnanski, I., Katz, Y., and Horev, E., "On the applicability of various scaling laws to the turbulent wall jet," *Journal of Fluid Mechanics*, Vol. 234, 1992, p. 669–690. https://doi.org/10.1017/S002211209200096X.

[2] Oerlemans, S., "Wind turbine noise: primary noise sources," 2011. https://doi.org/NLR-TP-2011-066.

[3] Doolan, C. J., Moreau, D. J., and Brooks, L. A., "Wind turbine noise mechanisms and some concepts for its control," *Acoustics Australia*, Vol. 40, No. 1, 2012. https://doi.org/https://hdl.handle.net/2440/71859.

[4] Brooks, T. F., and Hodgson, T., "Trailing edge noise prediction from measured surface pressures," *Journal of sound and vibration*, Vol. 78, No. 1, 1981, pp. 69–117. https://doi.org/10.1016/S0022-460X(81)80158-7.

[5] Brooks, T. F., Pope, D. S., and Marcolini, M. A., *Airfoil self-noise and prediction*, Vol. 1218, National Aeronautics and Space Administration, Office of Management, 1989. https://doi.org/19890016302.

[6] Hersh, A. S., Soderman, P. T., and Hayden, R. E., "Investigation of acoustic effects of leading-edge serrations on airfoils," *Journal of Aircraft*, Vol. 11, No. 4, 1974, pp. 197–202. https://doi.org/10.2514/3.59219.

[7] Raupach, M., and Thom, A. S., "Turbulence in and above plant canopies," *Annual Review of Fluid Mechanics*, Vol. 13, No. 1, 1981, pp. 97–129. https://doi.org/1981.13:97-129.

[8] Poggi, D., and Katul, G., "Two-dimensional scalar spectra in the deeper layers of a dense and uniform model canopy," *Boundary-layer meteorology*, Vol. 121, No. 2, 2006, pp. 267–281. https://doi.org/10.1007/s10546-006-9075-3.

[9] Skudrzyk, E., and Haddle, G., "Noise production in a turbulent boundary layer by smooth and rough surfaces," *The Journal of the Acoustical Society of America*, Vol. 32, No. 1, 1960, pp. 19–34. https://doi.org/10.1121/1.1907871.

[10] Clark, I. A., Alexander, W. N., Devenport, W., Glegg, S., Jaworski, J. W., Daly, C., and Peake, N., "Bioinspired Trailing-Edge Noise Control," *AIAA Journal*, Vol. 55, No. 3, 2017, pp. 740–754. https://doi.org/10.2514/1.J055243.

[11] Arguillat, B., Ricot, D., Bailly, C., and Robert, G., "Measured wavenumber: Frequency spectrum associated with acoustic and aerodynamic wall pressure fluctuations," *The Journal of the Acoustical Society of America*, Vol. 128, No. 4, 2010, pp. 1647–1655. https://doi.org/10.1121/1.3478780.

[12] Wang, Y., Zhao, K., Lu, X.-Y., Song, Y.-B., and Bennett, G. J., "Bio-Inspired Aerodynamic Noise Control: A Bibliographic Review," *Applied Sciences*, Vol. 9, No. 11, 2019. https://doi.org/10.3390/app9112224, URL https://www.mdpi.com/2076-3417/9/11/2224.

[13] Kaimal, J. C., and Finnigan, J. J., *Atmospheric boundary layer flows: their structure and measurement*, Oxford university press, 1994. https://doi.org/10.1093/oso/9780195062397.001.0001.

[14] Finnigan, J., "Turbulence in Plant Canopies," *Annual Review of Fluid Mechanics*, Vol. 32, No. 1, 2000, pp. 519–571. https://doi.org/10.1146/annurev.fluid.32.1.519.

[15] BELCHER, S. E., JERRAM, N., and HUNT, J. C. R., "Adjustment of a turbulent boundary layer to a canopy of roughness elements," *Journal of Fluid Mechanics*, Vol. 488, 2003, p. 369–398. https://doi.org/10.1017/S0022112003005019.

[16] Moreau, D., Brooks, L., and Doolan, C., "On the noise reduction mechanism of a flat plate serrated trailing edge at low-to-moderate Reynolds number," *18th AIAA/CEAS aeroacoustics conference (33rd AIAA aeroacoustics conference)*, 2012, p. 2186. https://doi.org/10.2514/6.2012-2186.

[17] Moreau, D., and Doolan, C., "Noise-Reduction Mechanism of a Flat-Plate Serrated Trailing Edge," *AIAA Journal*, Vol. 51, 2013, pp. 2513 – 2522. https://doi.org/10.2514/1.J052436.

[18] Finez, A., Jacob, M., Jondeau, E., and Roger, M., "Broadband noise reduction with trailing edge brushes," *16th AIAA/CEAS aeroacoustics conference*, 2010, p. 3980. https://doi.org/10.2514/6.2010-3980.

[19] Howe, M. S., "Noise produced by a sawtooth trailing edge," *The Journal of the Acoustical Society of America*, Vol. 90, No. 1, 1991, pp. 482–487. https://doi.org/10.1121/1.401273.

[20] Afshari, A., Azarpeyvand, M., Dehghan, A. A., and Szőke, M., "Trailing Edge Noise Reduction Using Novel Surface Treatments," 2016. https://doi.org/10.2514/6.2016-2834.

[21] Jaworski, J. W., and Peake, N., "Aerodynamic noise from a poroelastic edge with implications for the silent flight of owls," *Journal of Fluid Mechanics*, Vol. 723, 2013, p. 456–479. https://doi.org/10.1017/jfm.2013.139.

[22] JIMÉNEZ, J., UHLMANN, M., PINELLI, A., and KAWAHARA, G., "Turbulent shear flow over active and passive porous surfaces," *Journal of Fluid Mechanics*, Vol. 442, 2001, p. 89–117. https://doi.org/10.1017/S0022112001004888.

[23] Graham, R. R., "The Silent Flight of Owls," *The Journal of the Royal Aeronautical Society*, Vol. 38, No. 286, 1934, p. 837–843. https://doi.org/10.1017/S0368393100109915.

[24] Thorpe, W., and Griffin, D., "Lack of ultrasonic components in the flight noise of owls," *Nature*, Vol. 193, No. 4815, 1962, pp. 594–595. https://doi.org/10.1038/193594b0.

[25] Kroeger, R. A., Grushka, H. D., and Helvey, T. C., "Low Speed Aerodynamics for Ultra-Quiet Flight," 1972. https://doi.org/AD0893426.

[26] Lilley, G., "A study of the silent flight of the owl," *4th AIAA/CEAS Aeroacoustics Conference*, 1998, p. 2340. https://doi.org/10.2514/6.1998-2340.

[27] Jaworski, J. W., and Peake, N., "Aeroacoustics of Silent Owl Flight," *Annual Review of Fluid Mechanics*, Vol. 52, No. 1, 2020, pp. 395–420. https://doi.org/10.1146/annurev-fluid-010518-040436.

[28] Chase, D., "Modeling the wavevector-frequency spectrum of turbulent boundary layer wall pressure," *Journal of Sound and Vibration*, Vol. 70, No. 1, 1980, pp. 29–67. https://doi.org/https://doi.org/10.1016/0022-460X(80)90553-2.

[29] Clark, I., Baker, D., Alexander, W. N., Devenport, W. J., Glegg, S. A., Jaworski, J., and Peake, N., *Experimental and Theoretical Analysis of Bio-Inspired Trailing Edge Noise Control Devices*, 2016, p. 3020. https://doi.org/10.2514/6.2016-3020.

[30] Bodling, A., and Sharma, A., "Noise Reduction Mechanisms due to Bio-Inspired Airfoil Designs," 2017. URL https://hal.archives-ouvertes.fr/hal-03004943.

[31] Agrawal, B. R., and Sharma, A., "Numerical investigations of bio-inspired blade designs to reduce broadband noise in aircraft engines and wind turbines," *54th AIAA aerospace sciences meeting*, 2016, p. 0760. https://doi.org/10.2514/6.2016-0760.

[32] Bodling, A., and Sharma, A., "Numerical investigation of noise reduction mechanisms in a bio-inspired airfoil," *Journal of Sound and Vibration*, Vol. 453, 2019. https://doi.org/10.1016/j.jsv.2019.02.004.

[33] Millican, A. J., Clark, I., Devenport, W. J., and Alexander, W. N., *Owl-Inspired Trailing Edge Noise Treatments: Acoustic and Flow Measurements*, 2017, p. 1177. https://doi.org/10.2514/6.2017-1177, URL https://arc.aiaa.org/doi/abs/10.2514/6.2017-1177.

[34] Afshari, A., Azarpeyvand, M., Dehghan, A. A., and Szoke, M., *Effects of Streamwise Surface Treatments on Trailing Edge Noise Reduction*, 2017, p. 3499. https://doi.org/10.2514/6.2017-3499.

[35] Afshari, A., Azarpeyvand, M., Dehghan, A. A., Szőke, M., and Maryami, R., "Trailing-edge flow manipulation using streamwise finlets," *Journal of Fluid Mechanics*, Vol. 870, 2019, p. 617–650. https://doi.org/10.1017/jfm.2019.249.

[36] Jacobs, R. G., and Durbin, P. A., "Shear sheltering and the continuous spectrum of the Orr–Sommerfeld equation," *Physics of Fluids*, Vol. 10, No. 8, 1998, pp. 2006–2011. https://doi.org/10.1063/1.869716.

[37] Jimenez, I., Glegg, S. A., and Devenport, W. J., "The effect of shear sheltering on trailing edge noise," *AIAA AVIATION 2020 FORUM*, 2020, p. 2515. https://doi.org/10.2514/6.2020-2515.

[38] Nurani Hari, N., Szoke, M., Devenport, W. J., and Glegg, S. A., "Understanding Pressure Shielding by Canopies," *AIAA Scitech 2021 Forum*, 2021, p. 0817. https://doi.org/10.2514/6.2021-0817.

[39] Gnanamanickam, E. P., Bhatt, S., Artham, S., and Zhang, Z., "Large-scale motions in a plane wall jet," *Journal of Fluid Mechanics*, Vol. 877, 2019, pp. 239–281. https://doi.org/10.1017/jfm.2019.559.

[40] Naqavi, I. Z., Tyacke, J. C., and Tucker, P. G., "Direct numerical simulation of a wall jet: flow physics," *Journal of Fluid Mechanics*, Vol. 852, 2018, pp. 507–542. https://doi.org/10.1017/jfm.2018.503.

[41] Gersten, K., "The asymptotic downstream flow of plane turbulent wall jets without external stream," *Journal of Fluid Mechanics*, Vol. 779, 2015, pp. 351–370. https://doi.org/10.1017/jfm.2015.409.

[42] George, W. K., Abrahamsson, H., Eriksson, J., Karlsson, R. I., Löfdahl, L., and Wosnik, M., "A similarity theory for the turbulent plane wall jet without external stream," *Journal of Fluid Mechanics*, Vol. 425, 2000, pp. 367–411. https://doi.org/10.1017/S002211200000224X.

[43] Katz, Y., Horev, E., and Wygnanski, I., "The forced turbulent wall jet," *Journal of Fluid Mechanics*, Vol. 242, 1992, pp. 577–609.

[44] Kleinfelter, A. W., Repasky, R., Hari, N., Letica, S., Vishwanathan, V., Organski, L., Schwaner, J., Alexander, W. N., and Devenport, W. J., "Development and Calibration of a new Anechoic Wall Jet Wind Tunnel," *AIAA Scitech 2019 Forum*, 2019, p. 1936. https://doi.org/10.2514/6.2019-1936.

[45] Grissom, D., Smith, B., Devenport, W., and Glegg, S., "Rough wall boundary layer noise," *12th AIAA/CEAS Aeroacoustics Conference (27th AIAA Aeroacoustics Conference)*, 2006, p. 2409. https://doi.org/10.2514/6.2006-2409.

[46] Devenport, W. J., Grissom, D. L., Alexander, W. N., Smith, B. S., and Glegg, S. A., "Measurements of roughness noise," *Journal of Sound and Vibration*, Vol. 330, No. 17, 2011, pp. 4250–4273. https://doi.org/10.1016/j.jsv.2011.03.017.

[47] Clark, I., Devenport, W. J., Jaworski, J., Daly, C., Peake, N., and Glegg, S. A., "The noise generating and suppressing characteristics of bio-inspired rough surfaces," *20th AIAA/CEAS aeroacoustics conference*, 2014, p. 2911. https://doi.org/10.2514/6.2014-2911.

[48] Smith, B. S., "Wall jet boundary layer flows over smooth and rough surfaces," Ph.D. thesis, Virginia Tech, 2008. URL http://hdl.handle.net/10919/27597.

[49] Awasthi, M., Devenport, W. J., Glegg, S. A., and Forest, J. B., "Pressure fluctuations produced by forward steps immersed in a turbulent boundary layer," *Journal of Fluid Mechanics*, Vol. 756, 2014, pp. 384–421. https://doi.org/10.1017/jfm.2014.405.

[50] Glegg, S., and Devenport, W., *Aeroacoustics of low Mach number flows: fundamentals, analysis, and measurement*, Academic Press, 2017. https://doi.org/10.1016/B978-0-12-809651-2.09991-4.

[51] Szoke, M., Nurani Hari, N., Devenport, W. J., Glegg, S. A., and Teschner, T.-R., "Flow Field Analysis Around Pressure Shielding Structures," *AIAA AVIATION 2021 FORUM*, 2021, p. 2293. https://doi.org/10.2514/6.2021-2293.

[52] Nurani Hari, N., Szoke, M., Devenport, W. J., Glegg, S. A., Priddin, M. J., and Ayton, L. J., "Surface Pressure Prediction for Bio-Inspired Unidirectional Canopies in Wall-jet Boundary Layers," *AIAA AVIATION 2021 FORUM*, 2021, p. 2262. https://doi.org/10.2514/6.2021-2262.

[53] Gonzalez, A., Glegg, S. A., Hari, N., and Devenport, W. J., "Fundamental Studies of the Mechanisms of Pressure Shielding," *25th AIAA/CEAS Aeroacoustics Conference*, 2019, p. 2403. https://doi.org/10.2514/6.2019-2403.

[54] Goody, M., "Empirical spectral model of surface pressure fluctuations," *AIAA journal*, Vol. 42, No. 9, 2004, pp. 1788–1794.

[55] Bradshaw, P., and Gee, M., "Turbulent wall jets with and without an external stream," 1960. https://doi.org/10.1.1.227.2288.

[56] Blake, W. K., "Turbulent boundary-layer wall-pressure fluctuations on smooth and rough walls," *Journal of Fluid Mechanics*, Vol. 44, No. 4, 1970, pp. 637–660. https://doi.org/10.1017/S0022112070002069.

[57] Amiet, R. K., "Noise due to turbulent flow past a trailing edge," *Journal of sound and vibration*, Vol. 47, No. 3, 1976, pp. 387–393. https://doi.org/10.1016/0022-460X(76)90948-2.

[58] Blake, W. K., *Mechanics of flow-induced sound and vibration, Volume 2: Complex flow-structure interactions*, Academic press, 2017. https://doi.org/978-0-12-809274-3.

[59] Grasso, G., Jaiswal, P., Wu, H., Moreau, S., and Roger, M., "Analytical models of the wall-pressure spectrum under a turbulent boundary layer with adverse pressure gradient," *Journal of Fluid Mechanics*, Vol. 877, 2019, pp. 1007–1062. https://doi.org/10.1017/jfm.2019.616.

[60] Joseph, L. A., "Pressure fluctuations in a high-Reynolds-number turbulent boundary layer over rough surfaces of different configurations," Ph.D. thesis, Virginia Tech, 2017. URL http://hdl.handle.net/10919/79630.